autophagic degradation of Keap1 and prevent oxidative liver damage. *Cell Metab* 17: 73–84, 2013
27. Myeku N, Figueiredo-Pereira ME: Dynamics of the degradation of ubiquitinated proteins by proteasomes and autophagy: Association with sequestosome 1/p62. *J Biol Chem* 286: 22426–22440, 2011
28. Susa K, Kita S, Iwamoto T, Yang SS, Lin SH, Ohta A, Sohara E, Rai T, Sasaki S, Alessi DR, Uchida S: Effect of heterozygous deletion of WNK1 on the WNK-OSR1/ SPAK-NCC/NKCC1/NKCC2 signal cascade in the kidney and blood vessels. *Clin Exp Nephrol* 16: 530–538, 2012
29. Thastrup JO, Rafiqi FH, Vitari AC, Pozo-Guisado E, Deak M, Mehellou Y, Alessi DR: SPAK/OSR1 regulate NKCC1 and WNK activity: Analysis of WNK isoform interactions and activation by T-loop trans-autophosphorylation. *Biochem J* 441: 325–337, 2012
30. Oi K, Sohara E, Rai T, Misawa M, Chiga M, Alessi DR, Sasaki S, Uchida S: A minor role of WNK3 in regulating phosphorylation of renal NKCC2 and NCC co-transporters in vivo. *Biol Open* 1: 120–127, 2012
31. Sohara E, Rai T, Yang SS, Ohta A, Naito S, Chiga M, Nomura N, Lin SH, Vandewalle A, Ohta E, Sasaki S, Uchida S: Acute insulin stimulation induces phosphorylation of the Na-Cl cotransporter in cultured distal mpkDCT cells and mouse kidney. *PLoS ONE* 6: e24277, 2011
32. Yang SS, Lo YF, Wu CC, Lin SW, Yeh CJ, Chu P, Sytwu HK, Uchida S, Sasaki S, Lin SH: SPAK-knockout mice manifest Gitelman syndrome and impaired vasoconstriction. *J Am Soc Nephrol* 21: 1868–1877, 2010
33. Ohta A, Rai T, Yui N, Chiga M, Yang SS, Lin SH, Sohara E, Sasaki S, Uchida S: Targeted disruption of the Wnk4 gene decreases phosphorylation of Na-Cl cotransporter, increases Na excretion and lowers blood pressure. *Hum Mol Genet* 18: 3978–3986, 2009

This article contains supplemental material online at http://jasn.asnjournals.org/lookup/suppl/doi:10.1681/ASN.2014070639/-/DCSupplemental.

BASIC RESEARCH www.jasn.org

Aberrant Glycosylation and Localization of Polycystin-1 Cause Polycystic Kidney in an AQP11 Knockout Model

Yuichi Inoue,* Eisei Sohara,* Katsuki Kobayashi,† Motoko Chiga,* Tatemitsu Rai,* Kenichi Ishibashi,‡ Shigeo Horie,§ Xuefeng Su,‖ Jing Zhou,‖ Sei Sasaki,* and Shinichi Uchida*

*Department of Nephrology, Graduate School of Medical and Dental Sciences, Tokyo Medical and Dental University, Tokyo, Japan; †Division of Molecular Genetics, Clinical Research Center, Chiba-East National Hospital, Chiba, Japan; ‡Department of Medical Physiology, Meiji Pharmaceutical University, Tokyo, Japan; §Department of Urology, Juntendo University School of Medicine, Tokyo, Japan; and ‖Renal Division, Department of Medicine, Brigham and Women's Hospital, Harvard Medical School, Boston, Massachusetts

ABSTRACT

We previously reported that disruption of the aquaporin-11 (AQP11) gene in mice resulted in cystogenesis in the kidney. In this study, we aimed to clarify the mechanism of cystogenesis in AQP11(−/−) mice. To enable the analyses of AQP11 at the protein level *in vivo*, AQP11 BAC transgenic mice (Tg^{AQP11}) that express 3×HA-tagged AQP11 protein were generated. This AQP11 localized to the endoplasmic reticulum (ER) of proximal tubule cells in Tg^{AQP11} mice and rescued renal cystogenesis in AQP11(−/−) mice. Therefore, we hypothesized that the absence of AQP11 in the ER could result in impaired quality control and aberrant trafficking of polycystin-1 (PC-1) and polycystin-2 (PC-2). Compared with kidneys of wild-type mice, AQP11(−/−) kidneys exhibited increased protein expression levels of PC-1 and decreased protein expression levels of PC-2. Moreover, PC-1 isolated from AQP11(−/−) mice displayed an altered electrophoretic mobility caused by impaired *N*-glycosylation processing, and density gradient centrifugation of kidney homogenate and *in vivo* protein biotinylation revealed impaired membrane trafficking of PC-1 in these mice. Finally, we showed that the Pkd1(+/−) background increased the severity of cystogenesis in AQP11(−/−) mouse kidneys, indicating that PC-1 is involved in the mechanism of cystogenesis in AQP11(−/−) mice. Additionally, the primary cilia of proximal tubules were elongated in AQP11(−/−) mice. Taken together, these data show that impaired glycosylation processing and aberrant membrane trafficking of PC-1 in AQP11(−/−) mice could be a key mechanism of cystogenesis in AQP11(−/−) mice.

J Am Soc Nephrol 25: 2789–2799, 2014. doi: 10.1681/ASN.2013060614

Aquaporin-11 (AQP11) is a membrane-channel protein. Although AQP11 is reported to be permeable to the water molecule,[1–3] the permeability of AQP11 to other solutes remains unclear. AQP11(−/−) mice die in the neonatal period because of renal failure and retarded growth.[4,5] Moreover, AQP11(−/−) mice develop renal cysts, suggesting that AQP11 can play a role in cystogenesis.[4,5] However, the mechanisms of cystogenesis in AQP11(−/−) mice have yet to be clarified. One of the reasons for the difficulties in investigating AQP11 has been the lack of a good antibody for detecting endogenous AQP11 in mouse tissues.

Autosomal dominant polycystic kidney disease (PKD) is the most common inherited renal disorder, occurring in 1:400 to 1:1000 live births. It is characterized by gradual renal cyst development

Received June 12, 2013. Accepted March 27, 2014.

Published online ahead of print. Publication date available at www.jasn.org.

Correspondence: Dr. Eisei Sohara, Department of Nephrology, Graduate School of Medical and Dental Sciences, Tokyo Medical and Dental University, 1-5-45 Yushima, Bunkyo-ku, Tokyo 113-8519, Japan. Email: esohara.kid@tmd.ac.jp

Copyright © 2014 by the American Society of Nephrology

and expansion, ultimately resulting in massive kidney enlargement and ESRD. Among autosomal dominant PKD patients, 85%–90% of cases result from mutations in the PKD1 gene, whereas another 10%–15% of cases are accounted for by mutations in the PKD2 gene. PKD1 encodes polycystin-1 (PC-1), a 462-kD, 4303–amino acid integral membrane protein with 11 transmembrane domains, a long extracellular N terminus with multiple binding domains, and a short cytoplasmic C terminus that interacts with multiple proteins, including the protein product of PKD2, polycystin-2 (PC-2).[6] PC-2 is a significantly smaller 110-kD protein with six transmembrane domains. PC-1 and PC-2 are located in the plasma membrane and cilia of renal epithelia.[6–8]

To enable the analyses of AQP11 in mice at the protein level *in vivo*, we generated AQP11 BAC transgenic mice (Tg^{AQP11}) that express AQP11 tagged with 3×hemagglutinin (HA) sequence at its N terminus and showed that AQP11 localizes to the endoplasmic reticulum (ER) of proximal tubule cells *in vivo*. Moreover, to investigate the mechanisms of cystogenesis in AQP11(−/−) mouse kidneys, we focused on PC-1 and PC-2. Impaired glycosylation processing and membrane trafficking of PC-1 in AQP11(−/−) mouse kidneys were found, which could represent a key mechanism of cyst formation in AQP11(−/−) mice.

RESULTS

Generation of 3×HA-Tagged AQP11 BAC Transgenic Mice

Transgenic mice that expressed N-terminal 3×HA-tagged AQP11 were generated. A BAC clone containing the whole exons of mouse AQP11 with its 60-kb promoter region was used. A 3×HA tag flanked by the N terminus of AQP11 was inserted in BAC (Figure 1A). As shown in Figure 1B, Southern blots were used to select founder transgenic mice, which were successfully bred to establish the low- and high-copy transgenic mouse lines. Genomic PCR was used for detection of transgene (Figure 1C). A Western blot of kidney homogenate probed with anti-HA antibody detected that the 3×HA-tagged AQP11 was expressed in the kidney, confirming that a 3×HA-tagged AQP11 transgenic mouse was generated (Figure 1D). Additionally, no significant differences in body weight were observed between wild-type mice and either low- or high-copy Tg^{AQP11} mice (Supplemental Figure 1).

3×HA-Tagged AQP11 Transgene Rescued Renal Cyst Formation and Retarded Growth in AQP11(−/−) Mice

To clarify that the 3×HA tag does not affect the function and subcellular localization of AQP11 *in vivo*, AQP11(−/−)Tg^{AQP11} mice, which express only 3×HA-tagged AQP11 protein, were generated. The 3×HA-tagged AQP11 transgene completely rescued renal cystogenesis in 3-week-old AQP11(−/−) mice

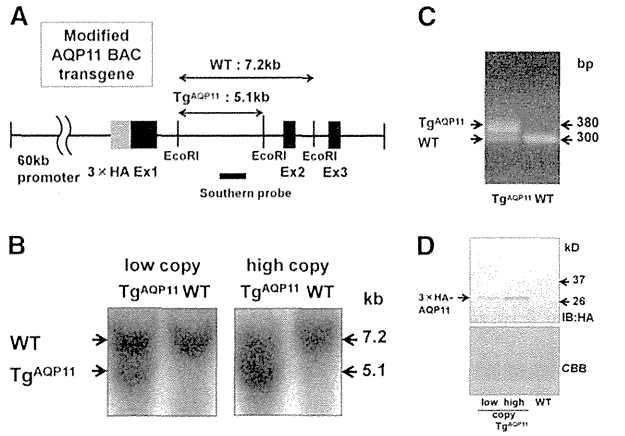

Figure 1. Generation of transgenic mice expressing 3×HA-tagged AQP11. (A) Structure of the modified AQP11 BAC transgene. 3×HA tag was fused to the N terminus of AQP11 in BAC. (B) Southern blot analysis of genomic DNA from wild-type (WT) and Tg^{AQP11} mice. (C) Genotyping analysis by PCR using genomic DNA derived from mouse tails. (D) Western blot of low- and high-copy Tg^{AQP11} mouse kidney homogenates probed with anti-HA antibody. 3×HA-AQP11 protein is indicated by arrows. Coomassie Brilliant Blue (CBB) staining was used as a loading control. IB, immunoblot.

(Figure 2, A and B, Supplemental Figure 2). Moreover, retarded growth in 3-week-old AQP11(−/−) mice was also rescued by the 3×HA-tagged AQP11 transgene (Figure 2C). These results showed that 3×HA-tagged AQP11 protein can function physiologically to replace native AQP11 protein *in vivo*.

Immunofluorescence of AQP11 in the Kidney

AQP11 localization in the Tg^{AQP11} mouse kidney was then examined. The immunofluorescence of Tg^{AQP11} mouse kidneys with anti-HA antibody revealed that AQP11 was present at the cortex, whereas no labeling was detected at the cortex of kidneys from wild-type littermates (Figure 3A). In the medulla, AQP11 labeling was absent in both wild-type and Tg^{AQP11} mice (Figure 3B). As shown in Figure 3C, double immunofluorescence with anti-HA and anti-AQP1 antibodies revealed that AQP11 was localized in the cytoplasm of proximal tubule cells. However, AQP11 staining was not detected in other segments of the kidney (Figure 3C), including the primary cilia. As expected from the observed proximal tubule localization of AQP11, the cysts in AQP11(−/−) mice originated mainly from the proximal tubules (Figure 3D).

AQP11 Localizes to ER *In Vivo*

To the best of our knowledge, the intracellular localization of AQP11 *in vivo* has yet to be reported. Double immunofluorescence with anti-HA antibody and organelle markers in the kidney revealed that 3×HA-tagged AQP11 was mainly colocalized with Lys-Asp-Glu-Leu (KDEL), an ER marker, and not with GM130, a Golgi marker, and Lamp2, a lysosome marker (Figure 4A). To confirm this ER localization of

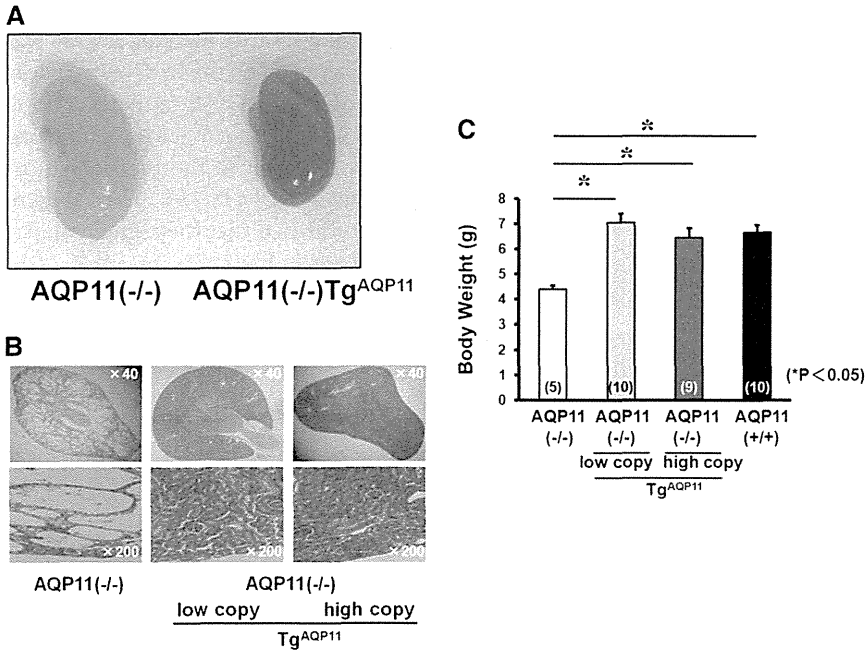

Figure 2. 3×HA-tagged AQP11 transgene rescued renal cyst formation and retarded growth in AQP11(−/−) mice. (A) Gross kidney and (B) histologic kidney sections of a 3-week-old AQP11(−/−) mouse and an AQP11(−/−)Tg^{AQP11} mouse. AQP11 transgene rescued renal cyst formation in AQP11(−/−) mice. (C) Body weight of 3-week-old AQP11(−/−), AQP11(−/−)Tg^{AQP11}, and AQP11(+/+) mice. AQP11 transgene rescued retarded growth in AQP11(−/−) mice. *P<0.05.

AQP11 *in vivo*, the ER fraction of the kidney was isolated from the Tg^{AQP11} mouse, and immunoblotting was performed. As shown in Figure 4B, robust expression of AQP11 was found in the ER fraction. These data clearly show ER localization of overexpressed transgenic AQP11 *in vivo*.

Loss of AQP11 Leads to Impaired Glycosylation Processing of PC-1

ER is the organelle that is involved in protein translation, translocation, protein folding, and *N*-glycosylation processing of many integral membrane proteins.[9] Because it is possible that AQP11 localizes to ER, we hypothesized that mechanisms of cystogenesis in the kidney of the AQP11(−/−) mouse were related to impaired quality control and aberrant trafficking of PC-1 and PC-2. PC-1 is a multidomain glycoprotein that is cleaved at a G protein–coupled receptor proteolytic site and divided into an N-terminal product (NTP) and a C-terminal product.[10] It has also been reported that mouse monoclonal antibody (7e12) detects endogenous PC-1 as two distinct glycoforms: endoglycosidase H-resistant (EndoH-resistant) and sensitive NTP forms.[11,12] As reported,[11,12] Western blot analyses of PC-1 with mouse monoclonal antibody (7e12) showed two NTP bands in mouse kidneys (Figure 5A). An increased protein expression level of PC-1 and a decreased protein expression level of PC-2 were also found in AQP11(−/−) mouse kidneys compared with wild-type mice (Figure 5). In addition, Western blot analyses of PC-1 detected an altered electrophoretic mobility of PC-1 in AQP11(−/−) mouse kidneys compared with wild-type mice, suggesting aberrant post-translational modification of PC-1, such as glycosylation (Figure 5A). In addition, the 3×HA-tagged AQP11 transgene rescued the altered electrophoretic mobility of PC-1 and the altered protein expression levels of PC-1 and PC-2 (Supplemental Figure 3). Therefore, to determine which type of protein modification is responsible for this altered electrophoretic mobility of PC-1, a deglycosylation assay was performed. Treatment of PC-1 with peptide-*N*-glycosidase F (PNGaseF), an enzyme that removes all N-linked sugars, reduced the size of the two products of abnormally modified PC-1 in AQP11(−/−) mice to the same molecular mass as the deglycosylated PC-1 product of wild-type mice (Figure 6A), indicating that PC-1 was abnormally *N*-glycosylated in AQP11(−/−) mouse kidneys. This abnormal *N*-glycosylation of PC-1 in AQP11(−/−) mouse kidneys was observed in the cortex but not the medulla (Supplemental Figure 4). In addition, we examined the effects of EndoH digestion on PC-1. EndoH resistance indicates the presence of mature complex glycans, which are typically required for protein trafficking to the cell surface. In wild-type mice, the upper PC-1 band was EndoH-resistant as previously reported (Figure 6A).[11] In contrast, in AQP11(−/−) mice, treatment with EndoH reduced the size of the abnormally glycosylated upper and lower bands, indicating that PC-1 from the AQP11(−/−) mouse kidney cortex is EndoH-sensitive (Figure 6A). These results suggested that the membrane trafficking of the abnormally glycosylated PC-1 in the AQP11(−/−) kidney was likely impaired. In contrast, the PNGaseF and EndoH assays on PC-2 and AQP1 showed no differences in molecular mass between wild-type and AQP11(−/−) mice before and after the treatment (Figure 6, B and C).

Impaired Membrane Trafficking of PC-1 in AQP11(−/−) Mouse Kidneys

Because PC-1 was found to be abnormally glycosylated in AQP11(−/−) mice, we hypothesized that membrane trafficking of PC-1 was impaired. To confirm this hypothesis, immunohistochemistry could not be used because of the lack of a good antibody. Therefore, ER and membrane compartments were prepared by density gradient centrifugation from wild-type and AQP11(−/−) kidney homogenates. Although PC-1 mainly localized at the ER, as previously

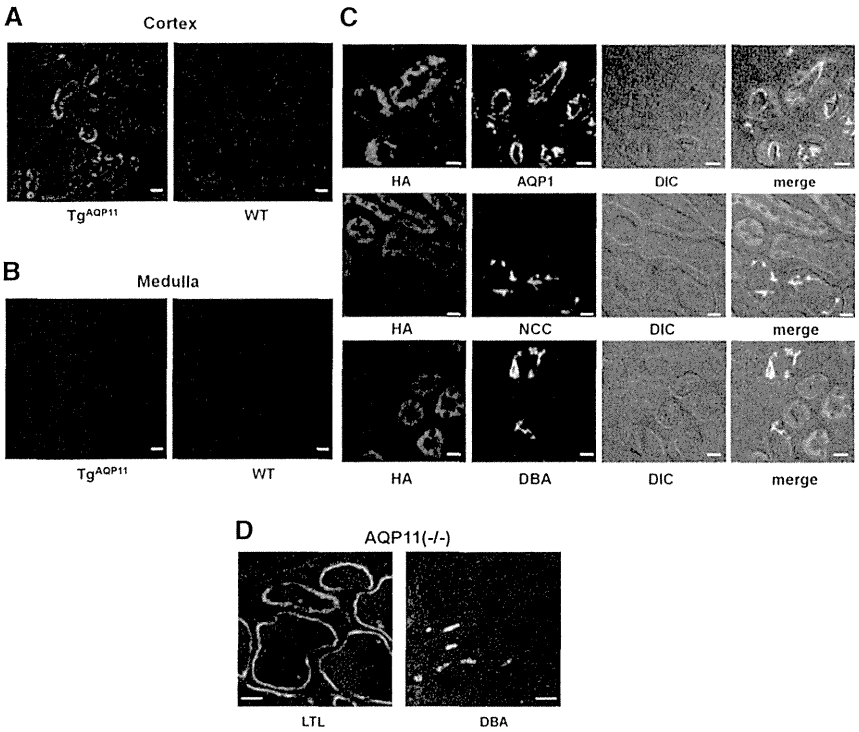

Figure 3. AQP11 protein expression in Tg^{AQP11} mouse kidney and the segmental origin of cysts in AQP11(−/−) mouse kidney. Immunofluorescence with HA antibody of 3-week-old Tg^{AQP11} and WT mouse kidneys: (A) cortex and (B) medulla. The immunostaining, image capture, and image processing were carried out under the same conditions. AQP11 was present only at the cortex. Scale bar, 20 μm. (C) Double immunofluorescence with HA antibody and AQP1 antibody (proximal tubule marker), NCC antibody (distal tubule marker), or dolichos biflorus agglutinin (DBA; collecting tubule and collecting duct marker) in the kidney of a 3-week-old Tg^{AQP11} mouse. AQP11 was localized in the cytoplasm of the proximal tubule cells. Scale bar, 10 μm. (D) Fluorescent staining with lotus tetragonolobus lectin (LTL; proximal tubule marker) and DBA in 3-week-old AQP11(−/−) mouse kidney. Segmental origin of cysts in AQP11(−/−) kidney was mainly proximal tubules. Scale bar, 50 μm.

reported,[13–15] protein expression of PC-1 in the plasma membrane fraction was clearly decreased in AQP11(−/−) mouse kidneys compared with wild-type mouse kidneys, suggesting that PC-1 trafficking to the plasma membrane was impaired (Figure 7, A and B). In addition, we used an *in vivo* protein biotinylation assay and showed that cell surface expression of PC-1 *in vivo* was clearly decreased in AQP11(−/−) kidneys compared with wild type (Figure 7C; Supplemental Figure 5). In contrast, membrane trafficking of PC-2 was still observed in AQP11(−/−) mice, although PC-2 levels in the membrane fraction were decreased (Supplemental Figure 6).

The Pkd1(+/−) Background Results in Increased Severity of PKD in the AQP11(−/−) Mouse

To confirm that loss of PC-1 function is a key mechanism involved in cystogenesis in AQP11(−/−) mice, the dosage of PC-1 was reduced using Pkd1(+/−) background in AQP11(−/−) mice. As expected, histologic examination of AQP11(−/−) mouse kidneys clearly revealed that the severity of cystic disease was markedly increased on the Pkd1(+/−) background in AQP11(−/−) littermates at postnatal day 12, indicating that loss of function of PC-1 is involved in the mechanism of cystogenesis in AQP11(−/−) mice (Figure 8A). We confirmed that the segmental origin of the cysts in Pkd1(+/−)AQP11(−/−) mice is mainly in the proximal tubules, consistent with AQP11(−/−) mice (Figure 8B). In addition, the kidney-to-body weight ratio (Figure 8C) and BUN (Figure 8D) showed significant increases in Pkd1(+/−) AQP11(−/−) mice compared with their counterparts.

Primary Cilia of Proximal Tubules Are Elongated in AQP11(−/−) Mice

Abnormal ciliary length has been reported in many renal cystic diseases.[11,16–21] Therefore, we examined the ciliary length of proximal tubules in AQP11(−/−) mice. Elongated primary cilia of proximal tubules were observed in AQP11(−/−) mice (Figure 9). In addition, 3×HA-tagged AQP11 transgene expression normalized the length of primary cilia in the AQP11(−/−) kidney, indicating that AQP11 may play a role in controlling ciliary length (Figure 9). However, the Pkd1(+/−) background did not alter the ciliary length of proximal tubules in AQP11(−/−) mice.

DISCUSSION

In this study, we generated Tg^{AQP11} mice to show that AQP11 localizes to the ER *in vivo*. Furthermore, we also confirmed that there were aberrant glycosylation processing and defective membrane trafficking of PC-1 in AQP11(−/−) mice, resulting in cyst formation in the kidney (Figure 10).

It is well known that PKD gene products localize to the primary cilia.[22] However, through the analysis of Tg^{AQP11} mice, AQP11 was found to be present in ER *in vivo* but not cilia. To date, only two nonciliary proteins other than AQP11 have been reported to be responsible for cystogenesis (glucosidase IIβ (GIIβ) and SEC63p) which are autosomal dominant polycystic liver disease–causing gene products. In ER, glycans are trimmed by glucosidases, and it has been reported that certain proteins fold improperly and fail to reach the Golgi in the absence of GII.[9] Loss of GIIβ and SEC63p led to cystogenesis in mouse liver and kidney.[22] Interestingly, both of them localize to ER as well as AQP11. GIIβ plays a role in

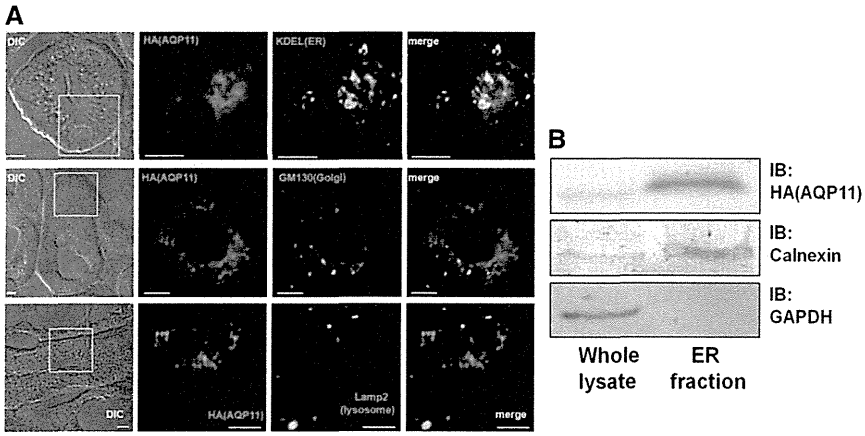

Figure 4. Subcellular localization of AQP11 in the Tg^{AQP11} mouse. (A) Immunofluorescence of Tg^{AQP11} mouse kidney with anti-HA antibody and organelle markers. The AQP11 immunostaining overlapped with KDEL (an ER marker) and not GM130, a Golgi marker, and Lamp2, a lysosome marker. Scale bar, 5 μm. (B) Immunoblotting analysis of the ER fraction from the Tg^{AQP11} mouse kidney. Calnexin was used as the ER marker. Robust expression of AQP11 was found in the ER.

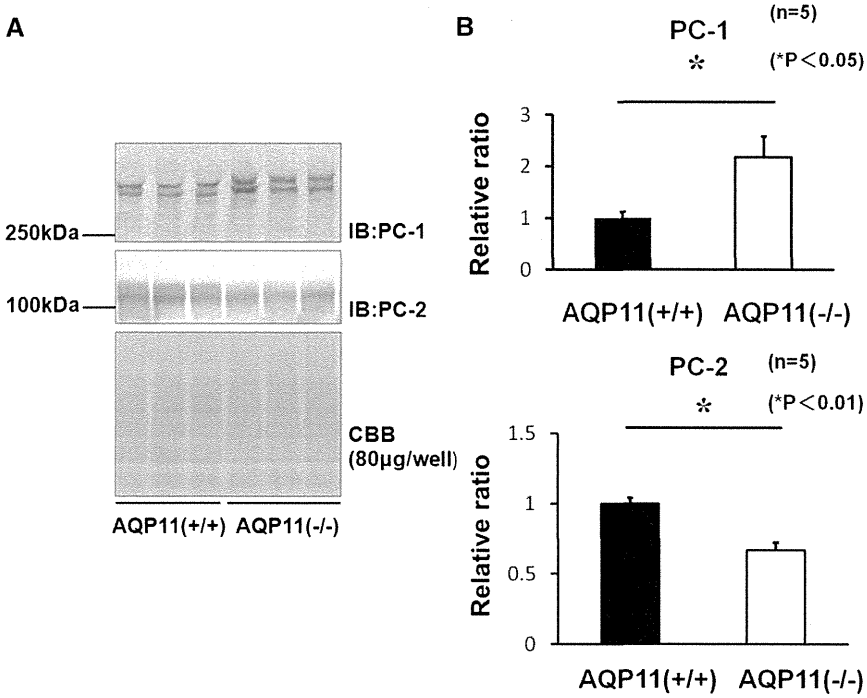

Figure 5. PC-1 and PC-2 in the AQP11(−/−) kidney. (A) Western blot of PC-1 and PC-2 in 2-week-old WT and AQP11(−/−) mouse kidneys. Western blot of PC-1 detected an altered electrophoretic mobility of PC-1 in AQP11(−/−) mouse kidneys compared with WT littermates, suggesting aberrant protein modification. (B) Densitometric analyses of PC-1 and PC-2 in AQP11(−/−) mouse kidneys. The relative levels of PC-1 and PC-2 expressions were determined by normalization to overall CBB staining in each lane. The PC-1 protein level in the kidneys of AQP11(−/−) mice was increased compared with that of WT littermates, and the PC-2 protein level in the kidneys of AQP11(−/−) mice was decreased compared with that of WT littermates. (Upper panel) *P<0.05. (Lower panel) *P<0.01.

glycosylation processing of PC-1 at the ER.[9,22] However, both kidney homogenates from GIIβ knockout mice and immortalized epithelial cells from kidney tubules of SEC63p knockout mice showed decreased protein expression of PC-1, which was opposite to the increased expression of PC-1 in AQP11(−/−) mice.[22] Although GIIβ protein was checked in AQP11(−/−) mouse kidneys, no difference was found in the GIIβ protein expression level in AQP11(−/−) mouse kidneys (data not shown). Taken together, AQP11 may play a role in glycosylation processing of PC-1 at the ER in a different manner from GIIβ and SEC63p. However, the reduction of EndoH-resistant PC-1 and impaired trafficking of PC-1 were observed in both AQP11(−/−) and GIIβ knockout mice.[22] It is possible that aberrantly glycosylated PC-1 in the AQP11(−/−) mouse is retained in the ER, similar to the GIIβ knockout mouse. Although PC-1 protein levels in the kidneys of AQP11(−/−) mice were increased, loss of function of PC-1, due to, impaired membrane localization, is considered to be the main cause of renal cystogenesis in AQP11(−/−) mice, which could represent a common mechanism of cystogenesis for ER proteins. In addition, PC-1 mRNA levels were not increased.[23] These data indicated that aberrantly glycosylated PC-1 might fail to enter the degradation pathway in AQP11(−/−) kidney because of the inability of PC-1 to exit the ER in the AQP11(−/−) kidney. Additional investigation will be required to clarify this issue.

In this study, it was shown that PCs are involved in the mechanism of cystogenesis in AQP11(−/−) mice; however, the true function of AQP11 at the ER remains unclear. It has been reported that proximal tubule cells exhibited ER vacuolization in AQP11(−/−) mouse kidneys.[4] In addition, increased ER stress response and oxidative stress in AQP11(−/−) mice were recently reported.[23–25] Therefore, AQP11 may play an important role in the homeostasis of the ER, and the absence of AQP11 could lead to ER dysfunction. However, to the best of our knowledge, there are no reports showing that renal cystogenesis is caused by nonspecific disruption of ER function. In this study, we clarified a

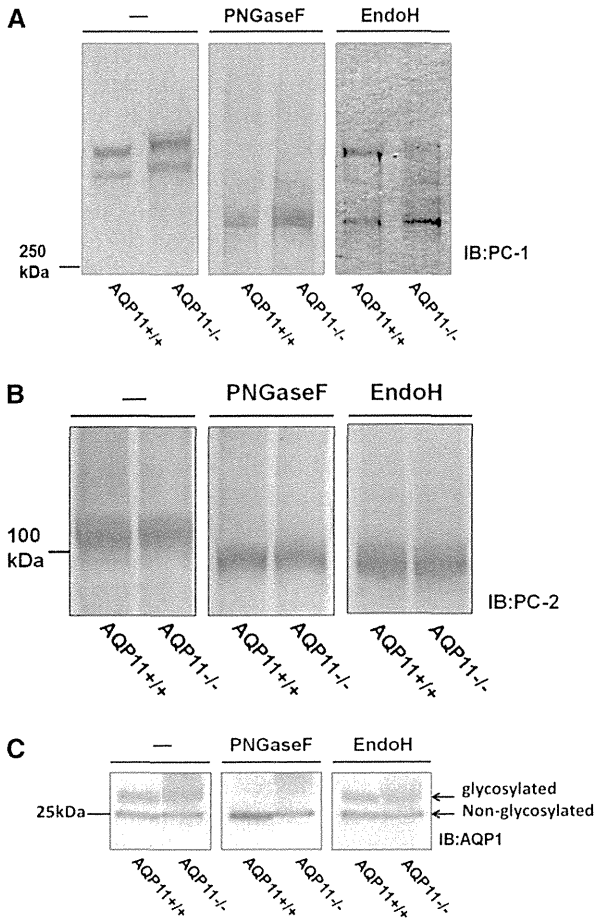

Figure 6. Aberrant glycosylation of PC-1 in AQP11(−/−) mouse kidney. (A) Treatment of PC-1 with PNGaseF reduced the size of the two products of abnormally modified PC-1 in AQP11(−/−) mice to the same molecular mass as the deglycosylated PC-1 product of WT mice. In addition, the upper PC-1 band in WT mice was EndoH-resistant, whereas the lower band was EndoH-sensitive. In contrast, the upper and lower bands in AQP11(−/−) kidney were EndoH-sensitive, with both bands being reduced in size to that of the EndoH-sensitive lower band from WT mice. (B) Treatment of PC-2 with PNGaseF and EndoH made no differences in molecular mass between WT and AQP11(−/−) mice both before and after treatment. To more readily detect the effect of deglycosylation, a greater amount of AQP11(−/−) kidney homogenate was loaded. (C) Treatment of AQP1 with PNGaseF and EndoH made no differences in molecular mass between WT and AQP11(−/−) mice both before and after treatment.

defective glycosylation in PC-1 in the proximal tubules of AQP11(−/−) mice but not other proteins, such as AQP1 and PC-2. Therefore, the absence of AQP11 in the ER might specifically lead to aberrant glycosylation of PC-1.

In this study, in contrast to PC-1, we observed decreased protein expression levels of PC-2 in the AQP11(−/−) kidney. It was previously reported that PC-2 mRNA levels are not altered significantly in AQP11(−/−) kidneys compared with wild type.[23] PC-2 could be misfolded, less stable, and susceptible to degradation because of the loss of AQP11 protein in the ER, and the mechanism of degradation for PC-1 and PC-2 could differ. In addition, although it is well known that inactivation of PKD2 leads to renal cystogenesis,[26–29] Wu *et al.*[26] reported that Pkd2(+/−) mice showed only limited renal cystogenesis in the age range of 9–17 weeks. Considering that the membrane trafficking of PC-2 is still observed in AQP11(−/−) mouse kidneys, the decreased PC-2 protein level in the kidneys of AQP11(−/−) mice at 2 weeks old might not be the main cause of renal cystogenesis in the AQP11(−/−) kidney. Additional investigation will be required.

Interestingly, although AQP11 does not localize to primary cilia, elongated primary cilia of proximal tubules in AQP11(−/−) mouse kidneys were observed (Figure 9). To the best of our knowledge, this case is the first in which ER protein was found to regulate the ciliary length of kidney tubules. Hopp *et al.*[11] recently reported that the ciliary length increase could be a compensatory response to reduced functional PC-1, suggesting that elongation of cilia is caused by loss of PC-1 function in AQP11(−/−) mice. However, the Pkd1(+/−) background did not change the ciliary length of proximal tubules in AQP11(−/−) mice (Figure 9). These data indicate that elongation of cilia in AQP11(−/−) mice might not be solely dependent on PC-1. In addition, these data also indicate that elongated primary cilia of proximal tubules in the kidneys of AQP11(−/−) mice might not play a major role in the mechanism of renal cystogenesis, although it is very interesting that an ER protein was found to regulate the ciliary length of kidney tubules. Additional investigation will be required.

In summary, impaired glycosylation processing and aberrant membrane trafficking of PC-1 could be key mechanisms of cystogenesis in AQP11(−/−) mice. The pathogenesis underlying PKD phenotypes remains unclear. It has been reported that aberrant PC-1 post-translational modifications, such as glycosylation, phosphorylation, and cleavage, are related to cyst formation.[10,22,30–33] Additional investigation of post-translational modifications of PC-1 will be required to clarify the pathogenesis of cystogenesis in PKD.

CONCISE METHODS

Mouse Lines

AQP11 BAC transgenic mice were generated by PhoenixBio (Utsunomiya, Tochigi, Japan). BMQ33M09, a 160-kb BAC clone containing the whole exons of mouse AQP11 with its promoter region was prepared. The galactokinase selection system was used for BAC recombineering,[34] and a 3×HA tag flanked by the N terminus of AQP11 of BAC was inserted. To select transgenic mice by Southern blotting and select AQP11(−/−)Tg^{AQP11} mice by PCR and *Eco*RI digestion, the modified BAC also contained a new *Eco*RI site in intron 1. The transgene was injected into fertilized eggs of C57BL/6J mice, and transgenic mice were obtained. Founder transgenic mice were identified by PCR and Southern blot analysis, and offspring were

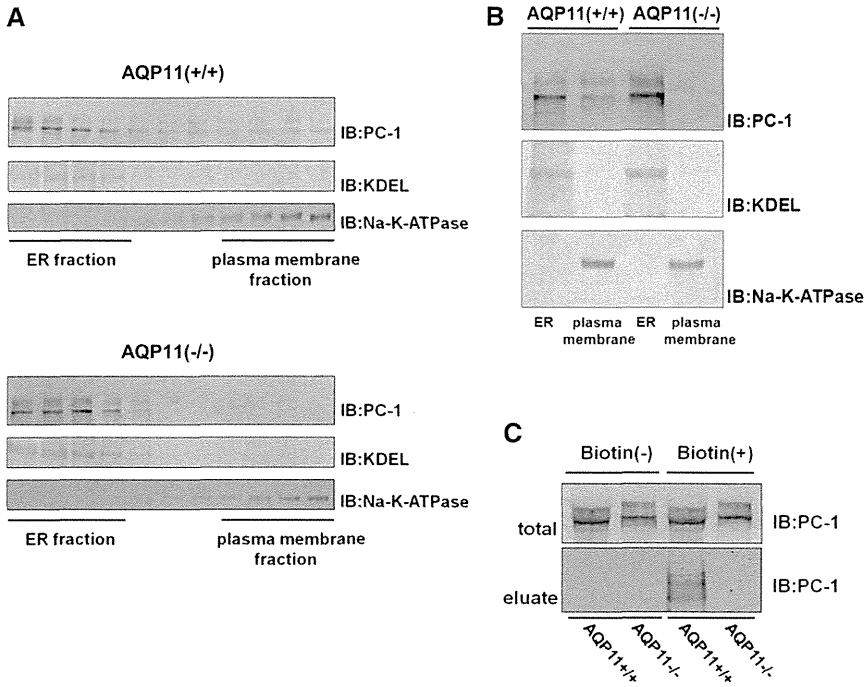

Figure 7. Impaired membrane trafficking of PC-1 in AQP11(−/−) mouse kidneys. After subcellular fractionation of kidney homogenates, samples of (A) individual fractions or (B) ER and plasma membrane fractions were analyzed by immunoblotting with antibodies against PC- 1, KDEL, and Na-K-ATPase. PC-1 protein expression in the plasma membrane fraction was clearly decreased in AQP11(−/−) kidneys compared with that of WT kidneys. (C) *In vivo* protein biotinylation showed that cell surface PC-1 protein expression *in vivo* was clearly decreased in AQP11(−/−) kidneys compared with WT.

genotyped by PCR. PCR primers were designed on both sides of the 3×HA tag. The forward primer was 5-AGGTCACATCTGCACAGCGC-3, the reverse primer was 5-ACGGGCCTGTGTAGCTGTTG-3, and the resulting amplification product was 380 bp. AQP11(+/−) mice[4] and Pkd1(+/−) mice[35,36] were used as previously reported. AQP11(−/−)Tg^{AQP11} mice were genotyped by PCR and *Eco*RI digestion. PCR primers were designed on both sides of the new *Eco*RI site. The forward primer was 5-TACTGCTGTGGCATGAGCAG-3 and the reverse primer was 5-GTTCCAAGGTATCCAGGGC-3. All animal studies were performed using the procedures approved by the Institutional Animal Care and Use Committee at the Tokyo Medical and Dental University.

Immunoblot Analyses

Kidneys were dissected as previously reported.[37] Kidney homogenates of 2-week-old mice without the nuclear fraction (600 g) were prepared to measure the levels of PC-1, PC-2, and AQP1. The crude membrane fractions (17,000-g pellet) of 3-week-old mouse kidneys were prepared to measure the levels of AQP11. Semiquantitative immunoblotting was performed as described previously.[38] The relative intensities of immunoblot bands were determined by densitometry with YabGelImage (free software). The primary antibodies used were rat anti-HA (Roche Applied Science, Penzberg, Germany), goat anticalnexin (Santa Cruz Biotechnology, Santa Cruz, CA), mouse anti-glyceraldehyde 3-phosphate dehydrogenase (Santa Cruz Biotechnology), mouse anti–PC-1 (7e12; Santa Cruz Biotechnology), rabbit anti–PC-2 (H-280; Santa Cruz Biotechnology), mouse anti-KDEL (Enzo Life Sciences, Farmingdale, NY), rabbit anti–Na-K-ATPase (Santa Cruz Biotechnology), rabbit anti-AQP1 (Sigma-Aldrich, St. Louis, MO), mouse anti-GM130 (BD Transduction Laboratories, San Jose, CA), guinea pig anti-NCC,[37] and rabbit anti–UT-A1 antibodies.[39] Alkaline phosphatase-conjugated anti-IgG antibodies (Promega, Madison, WI) and WesternBlue (Promega) were used to detect the signals. Deglycosylation assays by PNGaseF and EndoH (New England Biolab, Beverly, MA) were performed according to the manufacturer's protocol.

Immunohistochemical Analyses

Immunohistochemical analyses were performed on cryostat sections of Tg^{AQP11} and control littermate kidneys as well as formalin-fixed sections of AQP11(−/−) mice and their counterparts as previously reported.[40] The primary antibodies included rat anti-HA (Roche Applied Science), rabbit anti-HA (EMD Millipore, Billerica, MA), rabbit anti-AQP1 (Sigma-Aldrich), guinea pig anti-NCC,[37] mouse anti-KDEL (Enzo Life Sciences), mouse anti-GM130 (BD Transduction Laboratories), rat anti-Lamp2 (Developmental Studies Hybridoma Bank, Iowa City, IA), and mouse anti–α-acetylated tubulin (Sigma-Aldrich). Alexa fluor (Molecular Probes; Invitrogen, Carlsbad, CA) was used for secondary antibodies. Fluorescent *dolichos biflorus* agglutinin and *lotus tetragonolobus* lectin were purchased from Vector Laboratories (Burlingame, CA). Immunofluorescent images were obtained using an LSM510 laser-scanning confocal microscope system (Carl Zeiss, Oberkochen, Germany).

Isolation of ER from the Kidney

For detailed analysis of the intracellular localization of AQP11, ER was isolated from Tg^{AQP11} mouse kidneys, and immunoblotting was performed. To obtain the ER from the mouse kidneys, an ER extraction kit (Imgenex, San Diego, CA) was used following the manufacturer's instructions as previously reported.[41]

Subcellular Fractionation

Kidney lysates of 2-week-old mice were fractionated by density gradient centrifugation as previously reported.[13] After kidney homogenization in ice-cold homogenization buffer (250 mM sucrose, 1 mM EDTA, and 10 mM Tris-HCl, pH 7.5) containing protease inhibitors (protease inhibitor cocktail; Roche), a postnuclear supernatant was prepared by centrifugation at 1000 rpm for 10 minutes. Postnuclear supernatant was then layered onto a continuous 0%–15% Optiprep (Axis Shield PoC AS, Oslo,

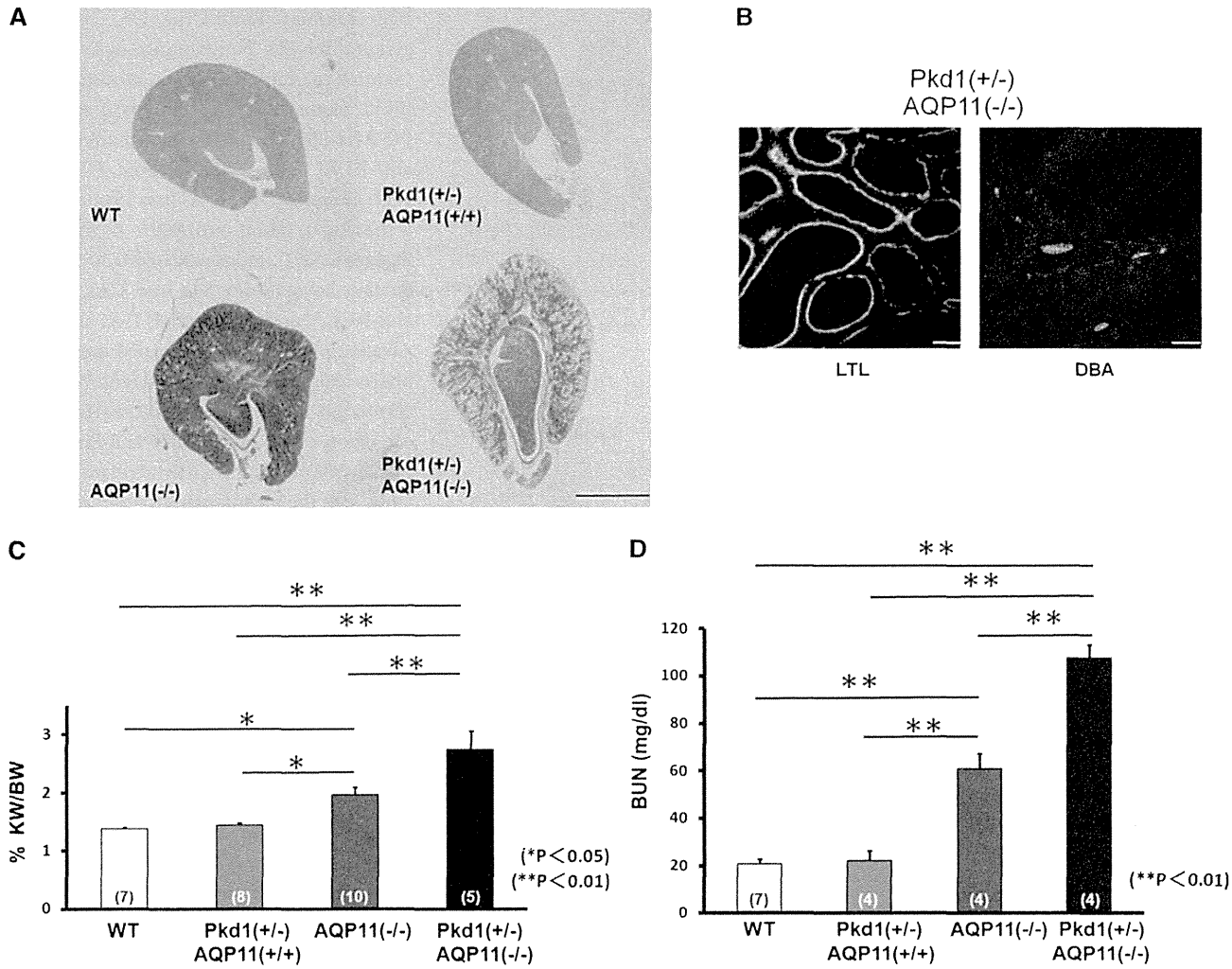

Figure 8. Pkd1(+/−) background resulted in increased severity of PKD in AQP11(−/−) mice. (A) Histologic kidney sections from littermates of the indicated genotypes at postnatal day 12. WT and Pkd1(+/−) mice showed no cysts. The Pkd1(+/−) background resulted in increased severity of PKD in AQP11(−/−) mice. Scale bar, 1 mm. (B) Fluorescent staining with LTL and DBA in 3-week-old Pkd1(+/−)AQP11(−/−) kidneys. The segmental origins of the cysts were mainly localized in the proximal tubules, which is consistent with AQP11(−/−) kidney. Scale bar, 50 μm. (C) The kidney-to-body weight ratio (KW/BW) and (D) BUN showed significant increases in Pkd1(+/−)AQP11(−/−) mice compared with their counterparts. *$P<0.05$; **$P<0.01$.

Norway) gradient and centrifuged at 200,000×*g* for 3 hours at 4°C using a swinging bucket rotor. The individual fractions were recovered from the top with a piston gradient fractionator. Equal amounts of samples were loaded and analyzed for PC-1, PC-2, KDEL, and Na-K-ATPase expressions. Finally, the ER and plasma membrane fractions were analyzed for PC-1, PC-2, KDEL, and Na-K-ATPase expressions.

In Vivo Protein Biotinylation

Proteins from 2-week-old mice were biotinylated *in vivo* as previously reported.[42] In brief, mice were anesthetized, the chest was opened, the left ventricle of the heart was punctured with a perfusion needle, and a small cut was made in the right atrium to allow outflow of the perfusion solutions. After blood components were washed away with prewarmed PBS supplemented with 10% (wt/vol) dextran 40 (GE Healthcare, Little Chalfont, United Kingdom), the mouse was perfused with biotinylation solution. The perfusion solution contained 1 mg/ml sulfo-NHS-LC-biotin (Pierce, Rockford, IL) in PBS (pH 7.4) and 10% (wt/vol) dextran 40. To neutralize unreacted biotinylation reagent, the mouse was then perfused with 50 mM Tris in PBS with 10% (wt/vol) dextran 40. After perfusion, kidneys were excised and freshly snap-frozen for preparation of organ homogenates. After homogenization with ice-cold homogenization buffer (1% Triton X-100, 150 mM NaCl, and 10 mM Tris-HCl, pH 7.5) containing protease inhibitor (protease inhibitor cocktail), homogenates were centrifuged at 16,100×*g* for 5 minutes at 4°C, and 3 mg total protein extract was added to a Streptavidin-Sepharose slurry (100 μl/sample; GE Healthcare). The biotinylated proteins were

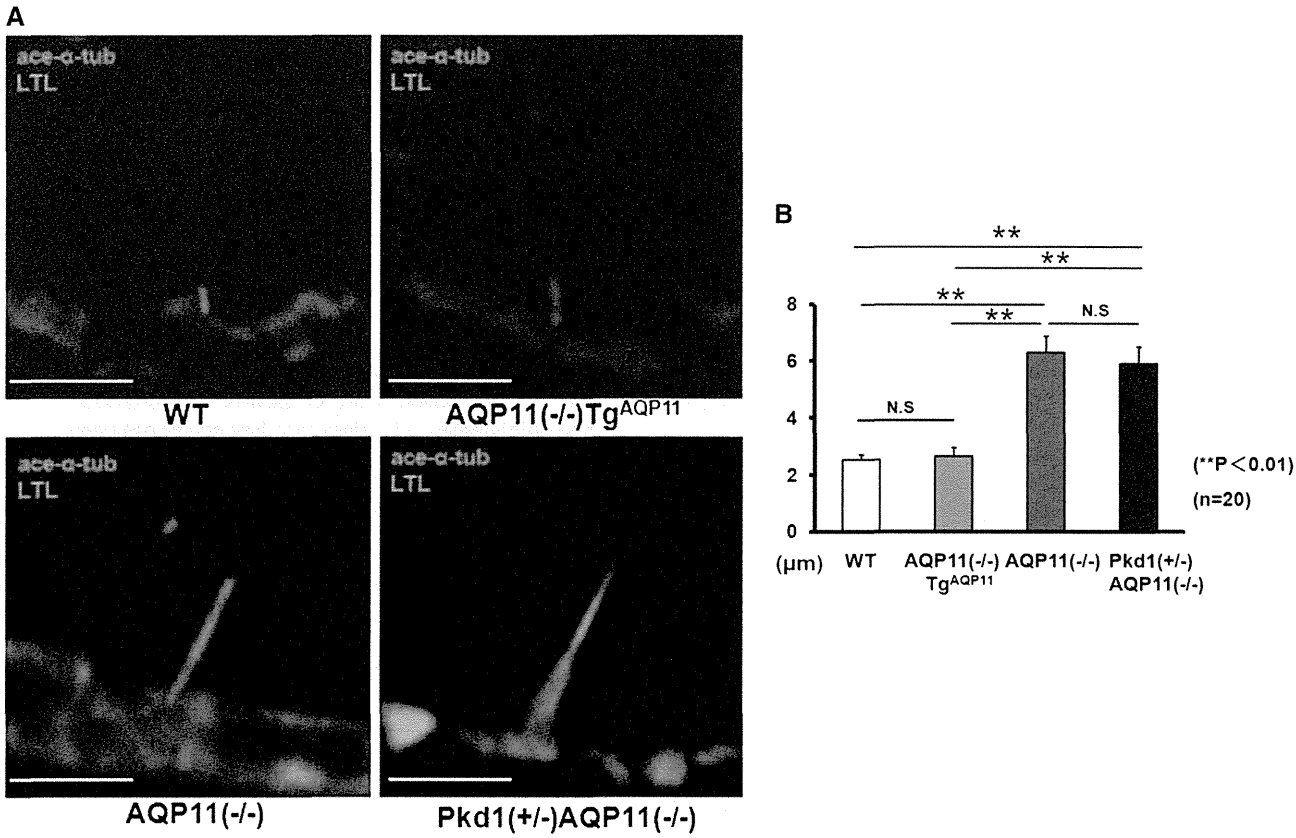

Figure 9. Primary cilia in proximal tubules were elongated in AQP11(−/−) mice. (A) Immunofluorescent labeling of kidney sections from 3-week-old WT, AQP11(−/−)Tg^{AQP11}, AQP11(−/−), and Pkd1(+/−)AQP11(−/−) mice with antiacetylated α-tubulin (red) and LTL (green). Scale bar, 5 μm. (B) Quantification of cilia length in kidney sections. The cilia lengths of proximal tubules in AQP11(−/−) and Pkd1(+/−)AQP11(−/−) mice were significantly longer than in WT mice. In addition, Tg^{AQP11} rescued abnormal ciliary length in AQP11 (−/−) mice. **$P<0.01$.

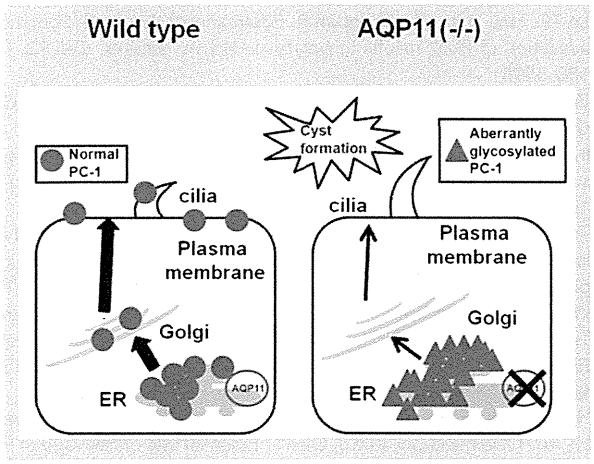

Figure 10. Schematic illustration of the mechanism of renal cystogenesis in the AQP11(−/−) kidney. Aberrant glycosylation processing and defective membrane trafficking of PC-1 in AQP11 (−/−) mice resulted in kidney cyst formation.

captured overnight at 4°C in a rotating mixer. The resin was washed three times and resuspended in 100 μl 2× SDS sample buffer at 60°C for 30 minutes.

Statistical Analyses

Comparisons between the two groups were performed using unpaired *t* tests. An ANOVA with Tukey *post hoc* test was used to evaluate significance in comparisons among multiple groups. *P* values <0.05 were considered significant. Data are presented as means±SEMs.

ACKNOWLEDGMENTS

We thank C. Iijima for help in the experiments.

This study was supported, in part, by Grants-in-Aid for Scientific Research (S, A) from the Japan Society for the Promotion of Science; a Grant-in-Aid for Young Scientists (B) from the Ministry of Education, Culture, Sports, Science and Technology of Japan; a Health and Labor Sciences Research Grant from the Ministry of Health, Labor, and Welfare; Salt Science Research Foundation Grant

1228; the Takeda Science Foundation; and a Banyu Foundation Research Grant.

DISCLOSURES

None.

REFERENCES

1. Yakata K, Hiroaki Y, Ishibashi K, Sohara E, Sasaki S, Mitsuoka K, Fujiyoshi Y: Aquaporin-11 containing a divergent NPA motif has normal water channel activity. *Biochim Biophys Acta* 1768: 688–693, 2007
2. Yakata K, Tani K, Fujiyoshi Y: Water permeability and characterization of aquaporin-11. *J Struct Biol* 174: 315–320, 2011
3. Ikeda M, Andoo A, Shimono M, Takamatsu N, Taki A, Muta K, Matsushita W, Uechi T, Matsuzaki T, Kenmochi N, Takata K, Sasaki S, Ito K, Ishibashi K: The NPC motif of aquaporin-11, unlike the NPA motif of known aquaporins, is essential for full expression of molecular function. *J Biol Chem* 286: 3342–3350, 2011
4. Morishita Y, Matsuzaki T, Hara-chikuma M, Andoo A, Shimono M, Matsuki A, Kobayashi K, Ikeda M, Yamamoto T, Verkman A, Kusano E, Ookawara S, Takata K, Sasaki S, Ishibashi K: Disruption of aquaporin-11 produces polycystic kidneys following vacuolization of the proximal tubule. *Mol Cell Biol* 25: 7770–7779, 2005
5. Tchekneva EE, Khuchua Z, Davis LS, Kadkina V, Dunn SR, Bachman S, Ishibashi K, Rinchik EM, Harris RC, Dikov MM, Breyer MD: Single amino acid substitution in aquaporin 11 causes renal failure. *J Am Soc Nephrol* 19: 1955–1964, 2008
6. Zhou J: Polycystins and primary cilia: Primers for cell cycle progression. *Annu Rev Physiol* 71: 83–113, 2009
7. Ibraghimov-Beskrovnaya O, Dackowski WR, Foggensteiner L, Coleman N, Thiru S, Petry LR, Burn TC, Connors TD, Van Raay T, Bradley J, Qian F, Onuchic LF, Watnick TJ, Piontek K, Hakim RM, Landes GM, Germino GG, Sandford R, Klinger KW: Polycystin: In vitro synthesis, in vivo tissue expression, and subcellular localization identifies a large membrane-associated protein. *Proc Natl Acad Sci U S A* 94: 6397–6402, 1997
8. Yoder BK, Hou X, Guay-Woodford LM: The polycystic kidney disease proteins, polycystin-1, polycystin-2, polaris, and cystin, are co-localized in renal cilia. *J Am Soc Nephrol* 13: 2508–2516, 2002
9. Janssen MJ, Waanders E, Woudenberg J, Lefeber DJ, Drenth JP: Congenital disorders of glycosylation in hepatology: The example of polycystic liver disease. *J Hepatol* 52: 432–440, 2010
10. Qian F, Boletta A, Bhunia AK, Xu H, Liu L, Ahrabi AK, Watnick TJ, Zhou F, Germino GG: Cleavage of polycystin-1 requires the receptor for egg jelly domain and is disrupted by human autosomal-dominant polycystic kidney disease 1-associated mutations. *Proc Natl Acad Sci U S A* 99: 16981–16986, 2002
11. Hopp K, Ward CJ, Hommerding CJ, Nasr SH, Tuan HF, Gainullin VG, Rossetti S, Torres VE, Harris PC: Functional polycystin-1 dosage governs autosomal dominant polycystic kidney disease severity. *J Clin Invest* 122: 4257–4273, 2012
12. Kurbegovic A, Côté O, Couillard M, Ward CJ, Harris PC, Trudel M: Pkd1 transgenic mice: Adult model of polycystic kidney disease with extrarenal and renal phenotypes. *Hum Mol Genet* 19: 1174–1189, 2010
13. Newby LJ, Streets AJ, Zhao Y, Harris PC, Ward CJ, Ong AC: Identification, characterization, and localization of a novel kidney polycystin-1-polycystin-2 complex. *J Biol Chem* 277: 20763–20773, 2002
14. Chapin HC, Rajendran V, Caplan MJ: Polycystin-1 surface localization is stimulated by polycystin-2 and cleavage at the G protein-coupled receptor proteolytic site. *Mol Biol Cell* 21: 4338–4348, 2010
15. Grimm DH, Cai Y, Chauvet V, Rajendran V, Zeltner R, Geng L, Avner ED, Sweeney W, Somlo S, Caplan MJ: Polycystin-1 distribution is modulated by polycystin-2 expression in mammalian cells. *J Biol Chem* 278: 36786–36793, 2003
16. Pazour GJ, Dickert BL, Vucica Y, Seeley ES, Rosenbaum JL, Witman GB, Cole DG: Chlamydomonas IFT88 and its mouse homologue, polycystic kidney disease gene tg737, are required for assembly of cilia and flagella. *J Cell Biol* 151: 709–718, 2000
17. Lin F, Hiesberger T, Cordes K, Sinclair AM, Goldstein LS, Somlo S, Igarashi P: Kidney-specific inactivation of the KIF3A subunit of kinesin-II inhibits renal ciliogenesis and produces polycystic kidney disease. *Proc Natl Acad Sci U S A* 100: 5286–5291, 2003
18. Masyuk TV, Huang BQ, Ward CJ, Masyuk AI, Yuan D, Splinter PL, Punyashthiti R, Ritman EL, Torres VE, Harris PC, LaRusso NF: Defects in cholangiocyte fibrocystin expression and ciliary structure in the PCK rat. *Gastroenterology* 125: 1303–1310, 2003
19. Smith LA, Bukanov NO, Husson H, Russo RJ, Barry TC, Taylor AL, Beier DR, Ibraghimov-Beskrovnaya O: Development of polycystic kidney disease in juvenile cystic kidney mice: Insights into pathogenesis, ciliary abnormalities, and common features with human disease. *J Am Soc Nephrol* 17: 2821–2831, 2006
20. Cadieux C, Harada R, Paquet M, Côté O, Trudel M, Nepveu A, Bouchard M: Polycystic kidneys caused by sustained expression of Cux1 isoform p75. *J Biol Chem* 283: 13817–13824, 2008
21. Sohara E, Luo Y, Zhang J, Manning DK, Beier DR, Zhou J: Nek8 regulates the expression and localization of polycystin-1 and polycystin-2. *J Am Soc Nephrol* 19: 469–476, 2008
22. Fedeles SV, Tian X, Gallagher AR, Mitobe M, Nishio S, Lee SH, Cai Y, Geng L, Crews CM, Somlo S: A genetic interaction network of five genes for human polycystic kidney and liver diseases defines polycystin-1 as the central determinant of cyst formation. *Nat Genet* 43: 639–647, 2011
23. Okada S, Misaka T, Tanaka Y, Matsumoto I, Ishibashi K, Sasaki S, Abe K: Aquaporin-11 knockout mice and polycystic kidney disease animals share a common mechanism of cyst formation. *FASEB J* 22: 3672–3684, 2008
24. Atochina-Vasserman EN, Biktasova A, Abramova E, Cheng DS, Polosukhin VV, Tanjore H, Takahashi S, Sonoda H, Foye L, Venkov C, Ryzhov SV, Novitskiy S, Shlonimskaya N, Ikeda M, Blackwell TS, Lawson WE, Gow AJ, Harris RC, Dikov MM, Tchekneva EE: Aquaporin 11 insufficiency modulates kidney susceptibility to oxidative stress. *Am J Physiol Renal Physiol* 304: F1295–F1307, 2013
25. Rojek A, Füchtbauer EM, Füchtbauer A, Jelen S, Malmendal A, Fenton RA, Nielsen S: Liver-specific Aquaporin 11 knockout mice show rapid vacuolization of the rough endoplasmic reticulum in periportal hepatocytes after amino acid feeding. *Am J Physiol Gastrointest Liver Physiol* 304: G501–G515, 2013
26. Wu G, D'Agati V, Cai Y, Markowitz G, Park JH, Reynolds DM, Maeda Y, Le TC, Hou H Jr., Kucherlapati R, Edelmann W, Somlo S: Somatic inactivation of Pkd2 results in polycystic kidney disease. *Cell* 93: 177–188, 1998
27. Pei Y, Watnick T, He N, Wang K, Liang Y, Parfrey P, Germino G, St George-Hyslop P: Somatic PKD2 mutations in individual kidney and liver cysts support a "two-hit" model of cystogenesis in type 2 autosomal dominant polycystic kidney disease. *J Am Soc Nephrol* 10: 1524–1529, 1999
28. Torra R, Badenas C, San Millán JL, Pérez-Oller L, Estivill X, Darnell A: A loss-of-function model for cystogenesis in human autosomal dominant polycystic kidney disease type 2. *Am J Hum Genet* 65: 345–352, 1999
29. Wu G, Markowitz GS, Li L, D'Agati VD, Factor SM, Geng L, Tibara S, Tuchman J, Cai Y, Park JH, van Adelsberg J, Hou H Jr., Kucherlapati R, Edelmann W, Somlo S: Cardiac defects and renal failure in mice with targeted mutations in Pkd2. *Nat Genet* 24: 75–78, 2000
30. Yu S, Hackmann K, Gao J, He X, Piontek K, García-González MA, Menezes LF, Xu H, Germino GG, Zuo J, Qian F: Essential role of cleavage of Polycystin-1 at G protein-coupled receptor proteolytic site for kidney tubular structure. *Proc Natl Acad Sci U S A* 104: 18688–18693, 2007
31. Roitbak T, Ward CJ, Harris PC, Bacallao R, Ness SA, Wandinger-Ness A: A polycystin-1 multiprotein complex is disrupted in polycystic kidney disease cells. *Mol Biol Cell* 15: 1334–1346, 2004

32. Chauvet V, Tian X, Husson H, Grimm DH, Wang T, Hiesberger T, Igarashi P, Bennett AM, Ibraghimov-Beskrovnaya O, Somlo S, Caplan MJ: Mechanical stimuli induce cleavage and nuclear translocation of the polycystin-1 C terminus. *J Clin Invest* 114: 1433–1443, 2004
33. Low SH, Vasanth S, Larson CH, Mukherjee S, Sharma N, Kinter MT, Kane ME, Obara T, Weimbs T: Polycystin-1, STAT6, and P100 function in a pathway that transduces ciliary mechanosensation and is activated in polycystic kidney disease. *Dev Cell* 10: 57–69, 2006
34. Warming S, Costantino N, Court DL, Jenkins NA, Copeland NG: Simple and highly efficient BAC recombineering using galK selection. *Nucleic Acids Res* 33: e36, 2005
35. Muto S, Aiba A, Saito Y, Nakao K, Nakamura K, Tomita K, Kitamura T, Kurabayashi M, Nagai R, Higashihara E, Harris PC, Katsuki M, Horie S: Pioglitazone improves the phenotype and molecular defects of a targeted Pkd1 mutant. *Hum Mol Genet* 11: 1731–1742, 2002
36. Ahrabi AK, Terryn S, Valenti G, Caron N, Serradeil-Le Gal C, Raufaste D, Nielsen S, Horie S, Verbavatz JM, Devuyst O: PKD1 haploinsufficiency causes a syndrome of inappropriate antidiuresis in mice. *J Am Soc Nephrol* 18: 1740–1753, 2007
37. Nishida H, Sohara E, Nomura N, Chiga M, Alessi DR, Rai T, Sasaki S, Uchida S: Phosphatidylinositol 3-kinase/Akt signaling pathway activates the WNK-OSR1/SPAK-NCC phosphorylation cascade in hyperinsulinemic db/db mice. *Hypertension* 60: 981–990, 2012
38. Sohara E, Rai T, Yang SS, Ohta A, Naito S, Chiga M, Nomura N, Lin SH, Vandewalle A, Ohta E, Sasaki S, Uchida S: Acute insulin stimulation induces phosphorylation of the Na-Cl cotransporter in cultured distal mpkDCT cells and mouse kidney. *PLoS ONE* 6: e24277, 2011
39. Uchida S, Sohara E, Rai T, Ikawa M, Okabe M, Sasaki S: Impaired urea accumulation in the inner medulla of mice lacking the urea transporter UT-A2. *Mol Cell Biol* 25: 7357–7363, 2005
40. Sohara E, Rai T, Yang SS, Uchida K, Nitta K, Horita S, Ohno M, Harada A, Sasaki S, Uchida S: Pathogenesis and treatment of autosomal-dominant nephrogenic diabetes insipidus caused by an aquaporin 2 mutation. *Proc Natl Acad Sci U S A* 103: 14217–14222, 2006
41. Ohta E, Itoh T, Nemoto T, Kumagai J, Ko SB, Ishibashi K, Ohno M, Uchida K, Ohta A, Sohara E, Uchida S, Sasaki S, Rai T: Pancreas-specific aquaporin 12 null mice showed increased susceptibility to caerulein-induced acute pancreatitis. *Am J Physiol Cell Physiol* 297: C1368–C1378, 2009
42. Rybak JN, Ettorre A, Kaissling B, Giavazzi R, Neri D, Elia G: In vivo protein biotinylation for identification of organ-specific antigens accessible from the vasculature. *Nat Methods* 2: 291–298, 2005

This article contains supplemental material online at http://jasn.asnjournals.org/lookup/suppl/doi:10.1681/ASN.2013060614/-/DCSupplemental.

Human Molecular Genetics, 2014, Vol. 23, No. 19 **5052–5060**
doi:10.1093/hmg/ddu217
Advance Access published on May 12, 2014

Impaired degradation of WNK1 and WNK4 kinases causes PHAII in mutant KLHL3 knock-in mice

Koichiro Susa[1,†], Eisei Sohara[1,†,*], Tatemitsu Rai[1], Moko Zeniya[1], Yutaro Mori[1], Takayasu Mori[1], Motoko Chiga[1], Naohiro Nomura[1], Hidenori Nishida[1], Daiei Takahashi[1], Kiyoshi Isobe[1], Yuichi Inoue[1], Kenta Takeishi[1], Naoki Takeda[2], Sei Sasaki[1] and Shinichi Uchida[1]

[1]Department of Nephrology, Graduate School of Medical and Dental Sciences, Tokyo Medical and Dental University, 1-5-45 Yushima Bunkyo, Tokyo 113-8519, Japan and [2]Division of Transgenic Technology, Institute of Resource Development and Analysis, Kumamoto University, 2-2-1 Honjo Chuo Kumamoto, Kumamoto 860-0811, Japan

Received February 25, 2014; Revised April 19, 2014; Accepted May 5, 2014

Pseudohypoaldosteronism type II (PHAII) is a hereditary disease characterized by salt-sensitive hypertension, hyperkalemia and metabolic acidosis, and genes encoding with-no-lysine kinase 1 (WNK1) and WNK4 kinases are known to be responsible. Recently, Kelch-like 3 (KLHL3) and Cullin3, components of KLHL3-Cullin3 E3 ligase, were newly identified as responsible for PHAII. We have reported that WNK4 is the substrate of KLHL3-Cullin3 E3 ligase-mediated ubiquitination. However, WNK1 and Na–Cl cotransporter (NCC) were also reported to be a substrate of KLHL3-Cullin3 E3 ligase by other groups. Therefore, it remains unclear which molecule is the target(s) of KLHL3. To investigate the pathogenesis of PHAII caused by KLHL3 mutation, we generated and analyzed KLHL3$^{R528H/+}$ knock-in mice. KLHL3$^{R528H/+}$ knock-in mice exhibited salt-sensitive hypertension, hyperkalemia and metabolic acidosis. Moreover, the phosphorylation of NCC was increased in the KLHL3$^{R528H/+}$ mouse kidney, indicating that the KLHL3$^{R528H/+}$ knock-in mouse is an ideal mouse model of PHAII. Interestingly, the protein expression of both WNK1 and WNK4 was significantly increased in the KLHL3$^{R528H/+}$ mouse kidney, confirming that increases in these WNK kinases activated the WNK-OSR1/SPAK-NCC phosphorylation cascade in KLHL3$^{R528H/+}$ knock-in mice. To examine whether mutant KLHL3 R528H can interact with WNK kinases, we measured the binding of TAMRA-labeled WNK1 and WNK4 peptides to full-length KLHL3 using fluorescence correlation spectroscopy, and found that neither WNK1 nor WNK4 bound to mutant KLHL3 R528H. Thus, we found that increased protein expression levels of WNK1 and WNK4 kinases cause PHAII by KLHL3 R528H mutation due to impaired KLHL3-Cullin3-mediated ubiquitination.

INTRODUCTION

Pseudohypoaldosteronism type II (PHAII) is a hereditary disease characterized by salt-sensitive hypertension, hyperkalemia, and metabolic acidosis (1,2). Mutations in with-no-lysine kinase 1 (WNK1) and WNK4 genes were reported to be responsible for PHAII (3). It was previously demonstrated that the WNK kinase family phosphorylates and activates oxidative stress-responsive kinase 1 (OSR1) and STE20/ SPS1-related proline/alanine-rich kinase (SPAK) (4,5), and that activated OSR1/SPAK kinases could phosphorylate and activate Na–Cl cotransporter (NCC), constituting the WNK-OSR1/SPAK-NCC phosphorylation signaling cascade. This regulation of NCC by WNK-OSR1/SPAK signaling was confirmed *in vivo* using various genetically engineered mouse models (6–14). Through analysis of the WNK4 knock-in PHAII mouse model, constitutive activation of this WNK-OSR1/SPAK-NCC phosphorylation cascade in kidney was found to be the major pathogenic mechanism of PHAII.

Recently, two additional novel genes, Kelch-like 3 (KLHL3) and Cullin3, were identified as responsible for PHAII (15,16). KLHL3 is a member of the BTB–BACK–Kelch family, which are known as substrate adapters of Cullin3-based E3 ubiquitin ligase complexes (17–20). We and others have reported

*To whom correspondence should be addressed at: Eisei Sohara, Department of Nephrology, Graduate School of Medical and Dental Sciences, Tokyo Medical and Dental University, 1-5-45 Yushima Bunkyo, Tokyo 113-8519, Japan. Tel: +81-3-5803-5214; Fax: +81-3-5803-5215; Email: esohara.kid@tmd.ac.jp
†These authors contributed equally to this work.

© *The Author 2014. Published by Oxford University Press. All rights reserved.*
For Permissions, please email: journals.permissions@oup.com

Downloaded from http://hmg.oxfordjournals.org/ at Tokyo Medican and Dental University on April 13, 2015

that KLHL3 interacts with Cullin3 and WNK4, induces WNK4 ubiquitination and reduces WNK4 protein levels in cultured cells and *Xenopus laevis* oocytes (21–24). Interestingly, it was also reported that WNK1 could be a substrate of KLHL3-Cullin3 E3 ubiquitin ligase (21,24). Moreover, another group reported that KLHL3 was able to bind to NCC and regulate its intracellular localization in cultured cells (16). Therefore, it remains unclear which molecule involved in the pathogenesis of PHAII is the *in vivo* target of KLHL3. In addition, the above experiments were performed in cultured cells. Thus, it is necessary to clarify the role of KLHL3 mutation in PHAII pathogenesis *in vivo*.

In this study, to answer these questions, we generated KLHL3$^{R528H/+}$ knock-in mice that carry the same mutation as autosomal dominant type PHAII patients. This KLHL3$^{R528H/+}$ knock-in PHAII model mouse revealed that increased protein expression levels of WNK1 and WNK4 kinases, due to impaired binding of KLHL3 with WNK kinases, cause PHAII *in vivo*. These results also indicated that both WNK1 and WNK4 are physiologically regulated by KLHL3-Cullin3-mediated ubiquitination *in vivo*.

RESULTS

Generation of KLHL3$^{R528H/+}$ knock-in mice

KLHL3$^{R528H/+}$ knock-in mice were generated using homologous recombination in Baltha1 embryonic stem (ES) cells to create a mutant allele (25). Exon 15 of the Klhl3 gene was replaced by a cassette expressing a neomycin selective marker flanked by loxP sites, which was followed by the mutant exon 15 (R528H) (Fig. 1A). Recombinant ES cell clones were injected into morula to generate chimeric mice. The neo cassette was deleted by crossing the mutant KLHL3$^{flox/+}$ mice with CAG promoter-Cre transgenic mice. Successful generation of KLHL3$^{R528H/+}$ knock-in mice was confirmed by genomic sequencing (Fig. 1B–E). In addition to the generation of KLHL3$^{R528H/+}$ heterozygous mice, we generated KLHL3$^{R528H/R528H}$ homozygous mice to more readily detect the pathological effects of mutant KLHL3 R528H.

PHAII phenotypes of KLHL3$^{R528H/+}$ knock-in mice

There were no significant differences in body weight and physical appearance between KLHL3$^{R528H/+}$ and wild-type mice. To confirm the KLHL3$^{R528H/+}$ mouse as an accurate model of PHAII, we measured systolic blood pressure of mice fed a normal-salt diet. The systolic blood pressure in the KLHL3$^{R528H/+}$ mice fed a normal-salt diet did not differ from that of wild-type mice (Table 1). Since PHAII shows salt-sensitive hypertension, we then measured blood pressure in mice fed a high-salt diet, which revealed that a high-salt diet produced significantly higher systolic blood pressure in KLHL3$^{R528H/+}$ mice compared with wild-type mice (133.5 ± 1.6 mmHg versus 120.1 ± 5.1 mmHg, respectively; $n = 5$ and 4, $P < 0.05$). Moreover, as shown in Table 2, KLHL3$^{R528H/+}$ mice exhibited hyperkalemia and metabolic acidosis similar to PHAII patients. These data clearly indicate that the KLHL3$^{R528H/+}$ mouse is an ideal model of PHAII caused by KLHL3 mutation. The severity of hyperkalemia and metabolic acidosis was not changed under a high-salt diet (Supplementary Material, Fig. S1). We also performed blood pressure measurement and analysis of blood biochemical characteristics of KLHL3$^{R528H/R528H}$ homozygous knock-in mice (Tables 1 and 2). Although KLHL3$^{R528H/R528H}$ mice also exhibited salt-sensitive hypertension, hyperkalemia and metabolic acidosis, the blood pressure and blood biochemistries did not significantly differ from those of KLHL3$^{R528H/+}$ mice.

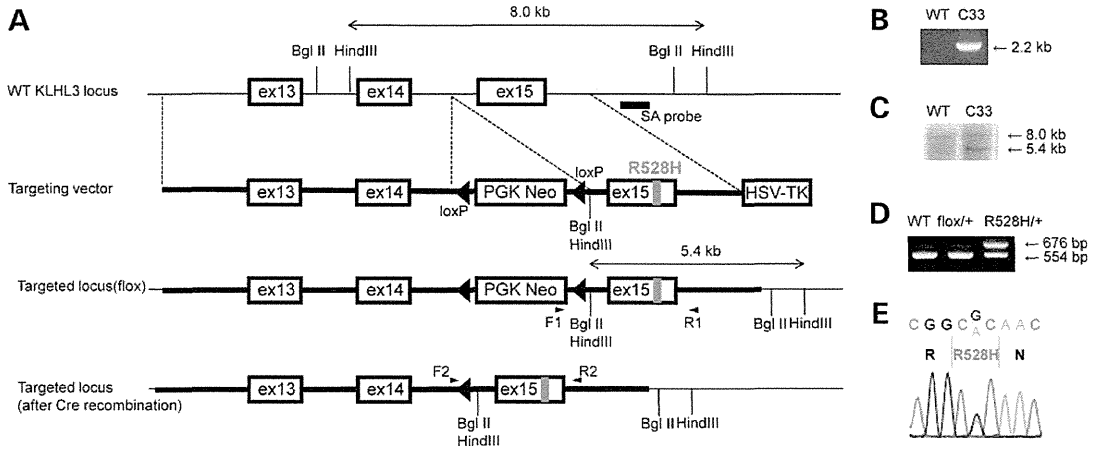

Figure 1. Generation of KLHL3$^{R528H/+}$ knock-in mice. (**A**) Targeting strategy for generating KLHL3$^{R528H/+}$ knock-in mice. The diagram shows the wild-type KLHL3 locus, the targeting construct and the targeted locus before and after Cre recombination. (**B**) Verification of homologous recombination by PCR of genomic DNA of the selected ES cell clones; primers F1 and R1 were as shown in (A). The 2.2 kb band is from the mutated allele. The primer set was designed to prevent amplification of the wild-type KLHL3 gene. C33 is the name of the selected ES cell clone. WT, host ES cells. (**C**) Verification of homologous recombination by Southern blotting of Hind III-digested genomic DNA derived from mouse tails. The 8.0 kb band is from the wild-type allele and the 5.4 kb band is from the mutated allele. (**D**) Genotyping PCR after Cre recombination using a primer set (F2 and R2) flanking the remaining loxP site. The 676 bp band represents the mutant allele containing the remaining loxP site, while the 554 bp band represents the wild-type allele. WT, wild-type mice; flox/+, KLHL3$^{flox/+}$ (R528H) mice; R528H/+, KLHL3$^{R528/+}$ mice. (**E**) Direct sequencing of the PCR product covering the mutation site.

Downloaded from http://hmg.oxfordjournals.org/ at Tokyo Medican and Dental University on April 13, 2015

Table 1. Blood pressure of wild-type, KLHL3$^{R528H/+}$, and KLHL3$^{R528H/R528H}$ mice

	WT	KLHL3$^{R528H/+}$	KLHL3$^{R528H/R528H}$
Systolic blood pressure (mmHg)			
Under normal diet	122.5 ± 2.0 ($n = 7$)	125.3 ± 3.0 ($n = 7$)	124.2 ± 1.6 ($n = 4$)
Under high-salt diet	120.1 ± 5.1 ($n = 4$)	133.5 ± 1.6* ($n = 5$)	136.3 ± 2.0* ($n = 4$)

*$P < 0.05$ compared with wild-type mice. No significant difference between KLHL$^{R528H/+}$ and KLHL3$^{R528H/R528H}$ mice was observed.

Table 2. Blood biochemical characteristics of wild-type, KLHL3$^{R528H/+}$, and KLHL3$^{R528H/R528H}$ mice

	WT	KLHL3$^{R528H/+}$	KLHL3$^{R528H/R528H}$
Blood biochemistries			
Na^+ (mmol/l)	149.0 ± 0.4	149.7 ± 0.4	149.9 ± 1.0
K^+ (mmol/l)	4.1 ± 0.1	4.8 ± 0.1*	4.8 ± 0.3*
Cl^- (mmol/l)	113.1 ± 0.4	116.0 ± 0.6*	115.8 ± 1.0*
BUN (mg/dl)	24.1 ± 1.4	22.9 ± 0.9	27.5 ± 2.4
Glu (mg/dl)	221.8 ± 8.3	219.3 ± 11.4	192.3 ± 17.9
pH	7.321 ± 0.008	7.287 ± 0.011*	7.261 ± 0.025*
pCO_2 (mmHg)	44.5 ± 1.4	46.1 ± 1.6	47.1 ± 3.1
$HCO3^-$ (mmol/l)	23.5 ± 0.4	21.7 ± 0.4*	20.7 ± 0.4*
Hb (g/dl)	14.7 ± 0.3 ($n = 12$)	14.6 ± 0.2 ($n = 12$)	14.5 ± 0.3 ($n = 8$)

BUN, blood urea nitrogen; Glu, glucose; Hb, hemoglobin. No significant difference between KLHL$^{R528H/+}$ and KLHL3$^{R528H/R528H}$ mice was observed in any values.
*$P < 0.05$ compared with wild-type mice.

Increased protein expression levels of WNK1 and WNK4 in KLHL3$^{R528H/+}$ mouse kidney

To investigate the pathogenesis of PHAII caused by the R528H mutation of KLHL3 *in vivo*, we examined the protein expression and phosphorylation of molecules constituting the WNK signaling pathway. As shown in Figure 2A and B, protein expression levels of WNK1 and WNK4 were significantly increased 1.8- and 1.4-fold, respectively, in the kidney of KLHL3$^{R528H/+}$ mice compared with those of wild-type mice. Accordingly, phosphorylation of OSR1, SPAK and NCC was also increased in KLHL3$^{R528H/+}$ mice. The KLHL3$^{R528H/R528H}$ homozygous mouse showed obvious increases of WNK1 and WNK4 protein levels (6.9- and 2.4-fold, respectively, compared with wild-type mice) and increased phosphorylation of OSR1 and SPAK. However, we also found that the protein level and the phosphorylation status of NCC in KLHL3$^{R528H/R528H}$ homozygous knock-in mice were not significantly increased compared with those in KLHL3$^{R528H/+}$ heterozygous knock-in mice, suggesting that the levels of increased WNK1 and WNK4 in the KLHL3$^{R528H/+}$ heterozygous knock-in mice might be high enough to fully phosphorylate and activate NCC. Considering that constitutive activation of NCC is the cause of PHAII, this saturated phosphorylation status of NCC could explain why the blood pressure and blood chemistries in KLHL3$^{R528H/R528H}$ homozygous knock-in mice did not differ from those of KLHL3$^{R528H/+}$ mice (Tables 1 and 2).

In addition, we confirmed that mRNA levels of WNK1 and WNK4 were not increased in the KLHL3$^{R528H/+}$ heterozygous mouse kidney (Fig. 2C), indicating that the increased protein levels of WNK1 and WNK4 were due to impaired degradation rather than transcriptional activation. To confirm that protein expression levels of WNK1 and WNK4 were increased in distal convoluted tubules (DCTs) where NCC is present, we performed double immunofluorescence of mouse kidney. As shown in Figure 3A and B, most of the KLHL3, WNK1 and WNK4 signals were colocalized with NCC, and signal intensities of WNK1 and WNK4 at DCT were apparently higher in the KLHL3$^{R528H/+}$ mouse kidney. Considering that both the WNK1 and WNK4 transgenic mice were reported to cause activation of the WNK-OSR1/SPAK-NCC phosphorylation cascade (9,21), these data clearly indicated that the essential pathogenesis of PHAII caused by KLHL3 mutation is due to increased WNK1 and WNK4 in DCT, leading to activation of the WNK-OSR1/SPAK-NCC phosphorylation signaling cascade.

Defective binding between the acidic motif of WNK1/WNK4 and mutant KLHL3 R528H

We had previously reported that KLHL3 mutation in the Kelch domain decreased its binding to the acidic domain of WNK4, leading to impaired ubiquitination and reduced WNK4 protein levels in HEK 293 cells (21). To confirm that the increased protein levels of WNK1 and WNK4 in KLHL3$^{R528H/+}$ mouse kidney were caused by impaired binding between WNK kinases and the mutant KLHL3 R528H, we measured the diffusion time of the TAMRA-labeled acidic motif of WNK1 or WNK4 peptide using fluorescence correlation spectroscopy (FCS) in the presence of different concentrations of GST-fusion proteins of wild-type and mutant KLHL3 R528H; the binding of KLHL3 to these peptides is observed as increased diffusion time of the fluorescent peptide (21,26,27). Wild-type KLHL3 increased the diffusion time of the TAMRA-labeled WNK1 and WNK4 peptides, confirming that wild-type KLHL3 can interact with the acidic motif of WNK1 as well as that of WNK4 (Fig. 4). On the

Downloaded from http://hmg.oxfordjournals.org/ at Tokyo Medican and Dental University on April 13, 2015

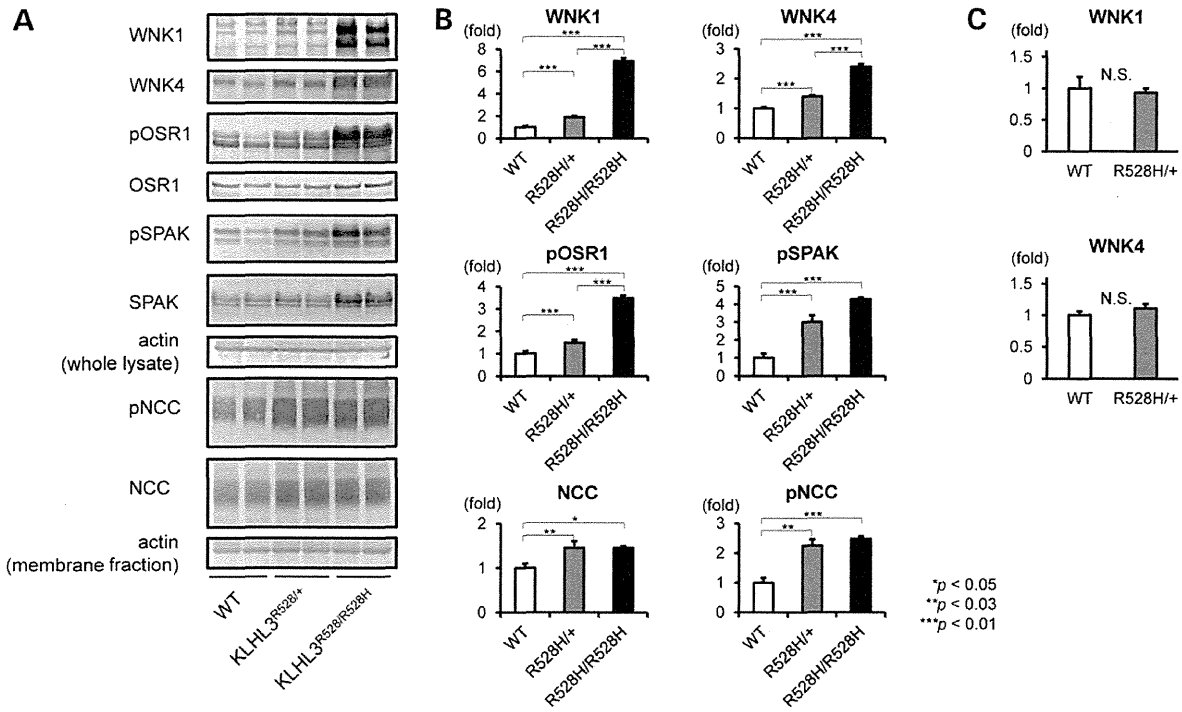

Figure 2. Increased WNK1 and WNK4 protein levels and activation of the WNK-OSR1/SPAK-NCC phosphorylation signaling cascade in KLHL3 mutant mouse kidney. (**A**) Representative immunoblots of the WNK-OSR1/SPAK-NCC signaling cascade in the kidneys of wild-type mice (WT), KLHL3$^{R528H/+}$ heterozygous knock-in mice and KLHL3$^{R528H/R528H}$ homozygous knock-in mice. (**B**) Densitometry analysis; values are expressed as a ratio of the average signal in wild-type mice. KLHL3$^{R528H/+}$ heterozygous knock-in mice and KLHL3$^{R528H/R528H}$ homozygous knock-in mice showed significantly increased protein levels of WNK1 and WNK4. The mutant KLHL3 mice also showed increased phosphorylation of OSR1, SPAK and NCC. WT, wild-type mice; R528H/+, KLHL3$^{R528/+}$ mice; R528H/R528H, KLHL3$^{R528/R528H}$ mice. $n = 6$ to 9. $^{*}P < 0.05$. $^{**}P < 0.03$. $^{***}P < 0.01$. (**C**) Quantitative PCR analysis of WNK1 and WNK4 mRNA levels. SYBR Green quantitative PCR was used to quantify mRNA levels in the kidneys of wild-type mice and KLHL3$^{R528H/+}$ mice. KLHL3$^{R528H/+}$ mice did not show significant differences of WNK1 and WNK4 mRNA levels in the kidney. WT, wild-type mice; R528H/+, KLHL3$^{R528/+}$ mice. $n = 5$.

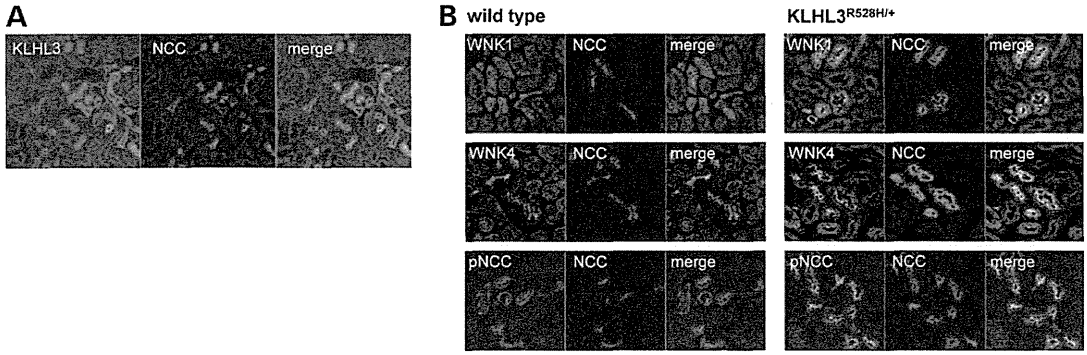

Figure 3. Immunofluorescence of WNK1, WNK4 and NCC in the kidney cortex. (**A**) Double immunofluorescence of KLHL3 and NCC in the kidney cortex of wild-type mice. The KLHL3 signal is colocalized with NCC. (**B**) Double immunofluorescence of WNK1 and NCC (upper), WNK4 and NCC (middle), and phosphorylated NCC and NCC (lower) in the kidney cortex of wild-type mice (left) and KLHL3$^{R528H/+}$ mice (right). Signals of WNK1, WNK4, NCC and pNCC are increased in KLHL3$^{R528H/+}$ mice.

other hand, the diffusion time of TAMRA-labeled WNK1 and WNK4 peptides was not affected by the addition of mutant KLHL3 R528H protein, indicating that neither WNK1 nor WNK4 bind to mutant KLHL3 R528H. The defective binding between WNK kinases and mutant KLHL3 R528H could result in impaired KLHL3-Cullin3 mediated ubiquitination of WNKs, as we previously reported, leading to increased protein expression of WNK kinases and activation of WNK signaling in the KLHL3$^{R528H/+}$ mouse kidney.

Regulation of epithelial Na^+ channels and ROMK in KLHL3$^{R528H/+}$ mice

We investigated epithelial Na^+ channels (ENaC) and renal outer medullary K^+ channels (ROMK), two important channels for Na^+ reabsorption and K^+ secretion in cortical collecting ducts (CCD), in KLHL3$^{R528H/+}$ mice. As shown in Figure 5, although KLHL3$^{R528H/+}$ mice did not show a significant change in the protein levels of total ENaC α subunit (85 kDa) compared

Downloaded from http://hmg.oxfordjournals.org/ at Tokyo Medican and Dental University on April 13, 2015

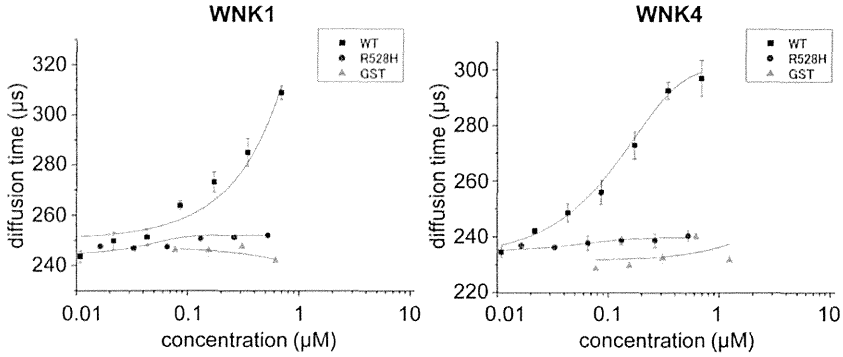

Figure 4. FCS assay of the binding between wild-type/mutant KLHL3 and WNK1/WNK4. The diffusion time of TAMRA-labeled WNK1 and WNK4 peptides containing the acidic motif was measured using FCS in the presence of different concentrations of GST fusion proteins of the wild-type KLHL3 and KLHL3 R528H mutant. The acidic motif of both WNK1 and WNK4 bound to the wild-type GST-KLHL3. On the other hand, GST alone and the KLHL3 R528H mutant did not affect the diffusion time, indicating that the KLHL3 R528H mutant could not bind to the acidic motif of WNK1 and WNK4.

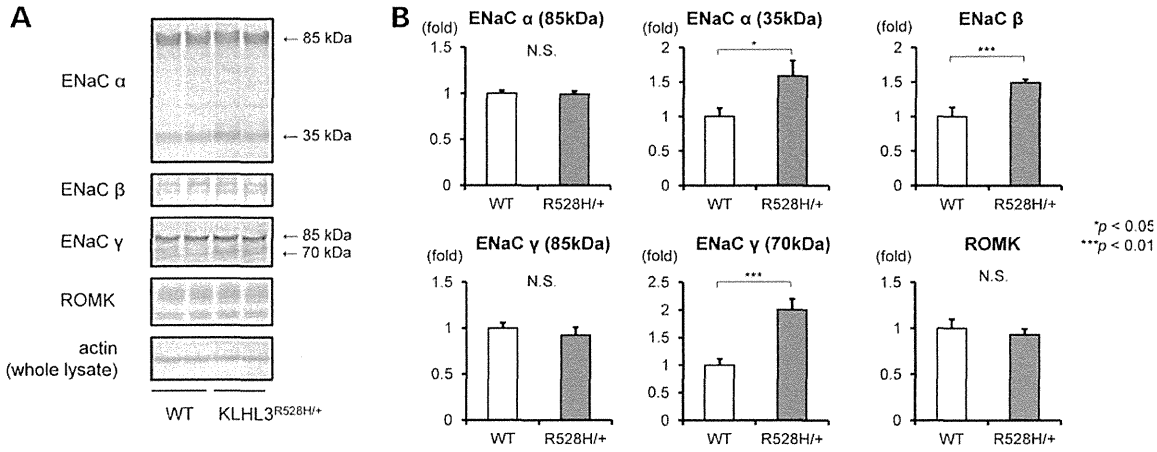

Figure 5. ENaC and ROMK in KLHL3$^{R528H/+}$ mice. (**A**) Representative immunoblots of ENaC α, ENaC β, ENaC γ subunits and ROMK in the kidneys of wild-type mice and KLHL3$^{R528H/+}$ mice. (**B**) Densitometry analysis of ENaC α, ENaC β, ENaC γ subunits and ROMK in the kidneys; values are expressed as a ratio of the average signal in wild-type mice. WT, wild-type mice; R528H/+, KLHL3$^{R528/+}$ mice. $n = 6$ to 9. $^{*}P < 0.05$. $^{***}P < 0.01$.

with wild-type mice, the levels of cleaved ENaC α subunit (35 kDa) were increased in KLHL3$^{R528H/+}$ mice. The level of ENaC β subunit was also increased in KLHL3$^{R528H/+}$ mice. Similar to ENaC α subunit, KLHL3$^{R528H/+}$ mice showed no significant change in the total protein level of ENaC γ subunit (85 kDa). However, a significant increase of cleaved ENaC γ subunit (70 kDa) was found in the KLHL3$^{R528H/+}$ mouse kidney. Similar to WNK4$^{D561A/+}$ knock-in mice (7), these results indicate that ENaC is activated in the KLHL3$^{R528H/+}$ mouse kidney. On the other hand, KLHL3$^{R528H/+}$ mice did not show a significant difference in protein levels of ROMK in immunoblot analysis of whole kidney (Fig. 5).

DISCUSSION

Investigation of the pathophysiology of PHAII is extremely important, not only to increase knowledge of this rare inherited disease, but also for the discovery of novel mechanisms of salt handling in the kidney. Although KLHL3 was identified as responsible for PHAII, several molecules have recently been reported as substrates that interact with KLHL3 in cultured cells. It was demonstrated that the loss of interaction between KLHL3 and WNK4 induced impaired ubiquitination of WNK4 and increased protein levels of WNK4 (21–24). In addition, WNK1 was also reported to be bound to KLHL3 (21,24). In contrast, Louis-Dit-Picard *et al.* (16) reported that KLHL3 is responsible for direct regulation of NCC membrane expression. Therefore, the pathophysiological role of KLHL3 in PHAII required investigation of *in vivo* kidney. For this purpose, we generated KLHL3$^{R528H/+}$ knock-in mice that carry a mutation found in human PHAII patients (15,16). This KLHL3$^{R528H/+}$ knock-in mouse exhibited salt-sensitive hypertension, hyperkalemia and metabolic acidosis, which are characteristic symptoms of PHAII patients. Moreover, increased NCC phosphorylation was also observed. These results clearly confirmed that our KLHL3$^{R528H/+}$ mouse is an ideal model of mutant KLHL3-induced PHAII.

To investigate the mechanisms of PHAII in KLHL3$^{R528H/+}$ mice, we assessed the protein levels and phosphorylation status of the WNK-OSR1/SPAK-NCC phosphorylation signaling cascade. Interestingly, KLHL3$^{R528H/+}$ heterozygous mice showed increased protein levels of both WNK1 and WNK4 in the kidney, and KLHL3$^{R528H/R528H}$ homozygous mice more

Downloaded from http://hmg.oxfordjournals.org/ at Tokyo Medican and Dental University on April 13, 2015

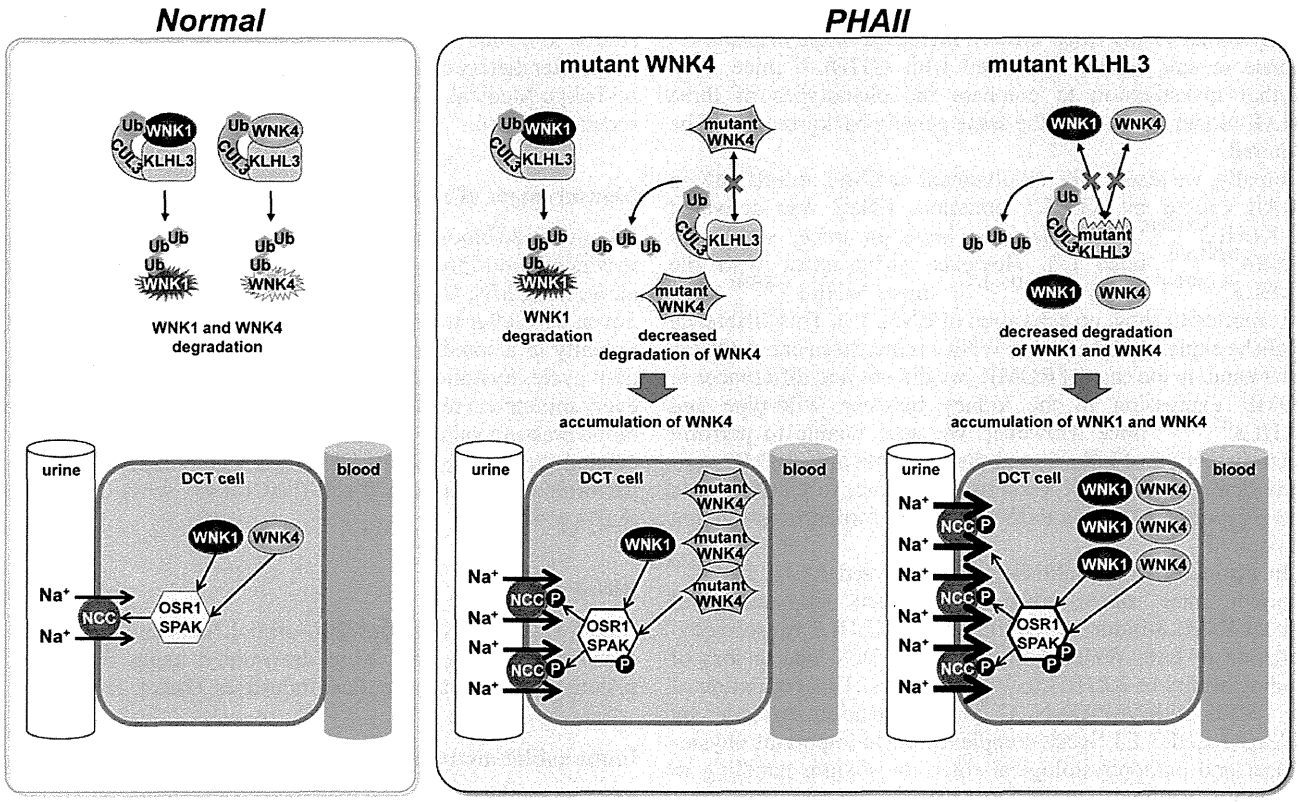

Figure 6. Schematic representation of the mechanism of PHAII caused by KLHL3 mutation.

clearly demonstrated increased WNK1 and WNK4 protein levels. We further demonstrated using an immunofluorescence assay that protein levels of both WNK1 and WNK4 are increased in DCT in KLHL3$^{R528H/+}$ mice. We also confirmed by FCS assay that mutant KLHL3 R528H did not bind to the acidic motif of either WNK1 or WNK4. Considering these observations, we have demonstrated for the first time that the essential mechanism of mutant KLHL3-induced PHAII involves impaired ubiquitination and increased protein levels of both of WNK1 and WNK4 in DCT *in vivo* (Fig. 6).

Importantly, these facts suggest that Cullin3-KLHL3 E3 ligase complexes physiologically regulate WNK-OSR1/SPAK-NCC phosphorylation cascades *in vivo*, indicating that KLHL3 plays an important role in the physiological mechanisms of sodium handling in the kidney. To date, physiological regulators of the WNK-OSR1/SPAK-NCC phosphorylation signal cascade, such as insulin (28–31), angiotensin II (10,32–34) and aldosterone (32,35–37), have been reported. However, the regulatory mechanism of these factors in WNK signaling remains unknown. The novel KLHL3-mediated regulation of WNK signals might be involved in these mechanisms. Further investigation is required to clarify this issue.

It was reported that KLHL3 was able to bind to NCC and regulate its intracellular localization in cultured cells (16). However, WNK and OSR1/SPAK were activated in KLHL3$^{R528H/+}$ mice, but were not down-regulated by increased NCC phosphorylation. Moreover, it was reported that simple over-expression of NCC did not produce the PHAII phenotype in NCC transgenic mice (38), indicating that increased phosphorylation, but not increased protein expression, of NCC is required for the PHAII phenotype *in vivo*. Considering these *in vivo* observations, the essential pathogenesis of PHAII caused by KLHL3 mutation is not due to impaired ubiquitination or regulation of NCC, but to the impaired ubiquitination of WNK kinases. This discrepancy could be due to the experimental system, the genetically engineered mouse model or cultured cells.

Boyden *et al.* (15) reported that symptoms of human PHAII patients caused by KLHL3 mutation are more severe than those caused by mutation in WNK1 or WNK4. WNK4$^{D561A/+}$ knock-in (7) and WNK1$^{+/FHHt}$ (9) PHAII mouse models exhibited increases of only a single kind of WNK kinase that carries a mutation. The increased severity of KLHL3 mutation-induced PHAII in human patients may be explained by the physiological difference between the increase of 'both WNK1 and WNK4 kinases' and 'a single WNK kinase'. Accumulation of both WNK1 and WNK4 kinases by KLHL3 mutation could result in further increases in phosphorylation of downstream components compared with the accumulation of a single WNK kinase (Fig. 6). However, the KLHL3$^{R528H/+}$ mouse shows a less severe phenotype than other mouse models of PHAII previously reported (7,9), which could be explained by the difference of origin of ES cells used for the generation of the knock-in mice, i.e. the difference of genetic background of these mice. In this study we utilized Baltha1 ES cells derived from C57BL/6 mouse, which is a one-renin-gene mouse strain. However, the other mouse models of PHA II were established with ES cells

Downloaded from http://hmg.oxfordjournals.org/ at Tokyo Medican and Dental University on April 13, 2015

derived from two-renin-gene mouse strains, 129Sv (7,9). It was reported that 129Sv mice showed increased blood pressure response to salt intake, compared with C57BL/6 mice (39). Further investigation to compare the phenotypes of three PHAII model mice under the same genetic background will be required.

Finally, we discuss the involvement of ENaC and ROMK in PHAII caused by KLHL3 mutation. ENaC was activated in KLHL3$^{R528H/+}$ heterozygous knock-in mice, similar to WNK4$^{D561A/+}$ mice (7). However, inconsistent with the KLHL3$^{R528H/+}$ and WNK4$^{D561A/+}$ mice, WNK1$^{+/FHHt}$ mice are reported to show no activation of ENaC (9). This difference might be explained by whether WNK4 is increased or not. On the other hand, in the case of ROMK, we did not find differences in ROMK expression in the kidney between wild-type and KLHL3$^{R528H/+}$ mice. However, we were unable to perform microdissection of kidney, and the available anti-ROMK antibody detects all ROMK variants. Therefore, to clarify the *in vivo* effect of KLHL3 on ROMK in CCD, further investigation is required.

In summary, we established and analyzed KLHL3$^{R528H/+}$ knock-in mice, and clarified the essential pathogenesis of mutant KLHL3-induced PHAII. Mutant KLHL3 causes accumulation of both WNK1 and WNK4 at DCT due to loss of binding ability of KLHL3 to WNK kinases. This regulation of the WNK-OSR1/SPAK-NCC phosphorylation cascade by Cullin3-KLHL3 E3 ligase complexes plays important physiological and pathophysiological roles for sodium handling in the kidney *in vivo*.

MATERIALS AND METHODS

Generation of KLHL3$^{R528H/+}$ knock-in mice

To generate KLHL3$^{R528/+}$ knock-in mice, the targeting vector was prepared using the BAC recombineering system (40). The point mutation (R528H) was introduced into exon 15 of the targeting vector by *galK* selection system (41). The targeting vector was then transfected into Baltha1 ES cells (25), which are derived from C57BL/6 mice, by electroporation as previously reported (42). After selection with 150 μg/ml G418 and 2 μM ganciclovir, targeted ES clones were selected by PCR with a sense primer F1 (5′-ATA GCA GAG CCG TCT CTG TG-3′) located within the neo cassette and an antisense primer R1 (5′-ACT TGT GTA GCG CCA AGT GC-3′) located following exon 15, Southern blotting and sequencing of the mutation site. Selected ES clones were injected into C57BL/6 morula. Chimeric males were bred with C57BL/6 females to produce mutant KLHL3$^{flox/+}$ (R528H) mice, and the neo cassette was then deleted by crossing these mutant KLHL3$^{flox/+}$ mice with transgenic mice expressing Cre recombinase under the control of the CAG promoter (43). Offsprings were genotyped by PCR with sense primer F2 (5′-CAC AGG GTA ACT GGG GCT GGT-3′) and antisense primer R2 (5′-GGA AGA ACT GTG ACC CCC GC-3′) flanking the remaining loxP site and exon 15.

Animals

Studies were performed using 10-week-old mice that had free access to food and water. Mice of each genotype were placed on a normal-salt diet (NaCl 0.4% w/w) or a high-salt diet (8.0% w/w) for 1 week. All experiments were performed 1 week after dietary change. The Animal Care and Use Committee of Tokyo Medical and Dental University approved the experimental protocol.

Measurement of blood pressure

We measured blood pressure by using a radiotelemetric method in which a blood pressure transducer (Data Sciences International, St. Paul, MN, USA) was inserted into the left carotid artery. Seven days after transplantation, each mouse was housed individually in a standard cage on a receiver under a 12 h light–dark cycle. Systolic and diastolic blood pressure was recorded every minute via radiotelemetry. For each mouse, we measured blood pressure values for more than 3 consecutive days and calculated the mean ± SE of all values. These experiments were performed under a normal-salt (NaCl 0.4% w/w) or high-salt (8.0% w/w) diet.

Blood analysis

Blood was drawn from the retro-orbital sinus under light ether anesthesia. Serum data were determined using the i-STAT system (FUSO Pharmaceutical Industries, Osaka, Japan).

Immunoblot analysis

Immunoblot analyses were performed on kidney homogenates. Kidneys were dissected from mice. Homogenates of whole kidney without the nuclear fraction (600 g) were prepared, and the crude membrane fraction (17 000 g) was used to measure the levels of NCC as described previously (7). Blots were probed with the following primary antibodies: anti-WNK1 (A301–516A; Bethyl, Montgomery, TX, USA), anti-WNK4 (36), anti-total OSR1 (M10; Abnova, Taipei, Taiwan), anti-phosphorylated OSR1 (44), anti-total SPAK (Cell Signaling Technology, Danvers, MA, USA), anti-phosphorylated SPAK (33), anti-total NCC (29), anti-phosphorylated NCC (pSer71) (28), anti-ENaC α subunit (kindly provided by M. Knepper), anti-ENaC β subunit (Alomone, Jerusalem, Israel), anti-ENaC γ subunit (kindly provided by M. Knepper), and anti-ROMK antibodies (kindly provided by J. B. Wade and P. A. Welling) (45), anti-actin (Cytoskeleton, Denver, CO, USA). Alkaline-phosphatase-conjugated anti-IgG antibodies (Promega, Madison, WI, USA) and Western Blue (Promega) were used to detect the signals. The relative intensities of immunoblot bands were determined by densitometry with YabGelImage free software.

Quantitative PCR analysis

Quantitative PCR analysis was performed on kidney as previously described (46). Total RNA from mouse kidneys was extracted using TRIzol reagent (Invitrogen, Carlsbad, CA, USA), according to the manufacturer's instructions. Total RNA was reverse transcribed using Omniscript reverse transcriptase (Qiagen, Hilden, Germany). Quantitative real-time PCR by Thermal Cycler Dice (Takara Bio, Otsu, Japan) was performed using the primer sets shown in a previous report (47).

Downloaded from http://hmg.oxfordjournals.org/ at Tokyo Medican and Dental University on April 13, 2015

Immunofluorescence

Kidneys were fixed by perfusion with periodate lysine (0.2 M) and paraformaldehyde (2%) in PBS. Immunofluorescence was performed as previously described (42). The primary antibodies used were anti-KLHL3 (Proteintech, Chicago, IL, USA), anti-WNK1 (A301–516A; BETHYL), anti-WNK4 (36), anti-NCC (29) and anti-pNCC (pSer71) (28). Alexa 488 or 546 dye-labeled (Molecular Probes; Invitrogen) secondary antibodies were used for immunofluorescence. Immunofluorescence images were obtained using an LSM510 Meta Confocal Microscope (Carl Zeiss, Oberkochen, Germany).

Fluorescence correlation spectroscopy

Fluorescent TAMRA-labeled WNK1 and WNK4 peptides covering the acidic motif were prepared (Hokkaido System Science Co., Ltd., Hokkaido, Japan). Human full-length KLHL3 (wild-type and R528H mutant) was cloned into pGEX6P-1 vectors. The recombinant GST-fusion KLHL3 protein expressed in BL21 *Escherichia coli* cells was purified using glutathione Sepharose beads. The TAMRA-labeled WNK peptides were incubated at room temperature for 30 min with different concentrations of GST-KLHL3 (0–2 μM) in 1× PBS containing 0.05% Tween 20 (reaction buffer). FCS measurements using the FluoroPoint-light analytical system (Olympus, Tokyo, Japan) were performed as previously described (26,27). The measurements were repeated five times per sample.

Statistics

Data are presented as means ± SE. A student's *t*-test was used for comparisons between groups. ANOVA and Tukey's test were used for multiple comparisons.

SUPPLEMENTARY MATERIAL

Supplementary Material is available at *HMG* online.

ACKNOWLEDGEMENTS

We thank C. Iijima for help in the experiments. We thank M. Knepper, J. B. Wade and P. A. Welling for provision of antibodies.

Conflict of Interest statement. The authors declare that they have no conflict of interest.

FUNDING

This study was supported, in part, by Grants-in-Aid for Scientific Research (S, A) from the Japan Society for the Promotion of Science; Grant-in-Aid for Young Scientists (B) from the Ministry of Education, Culture, Sports, Science and Technology of Japan; a Health and Labor Sciences Research Grant from the Ministry of Health, Labor and Welfare; the Salt Science Research Foundation (grant no. 1228); the Takeda Science Foundation; Banyu Foundation Research Grant and the Vehicle Racing Commemorative Foundation.

REFERENCES

1. Gordon, R.D. (1986) Syndrome of hypertension and hyperkalemia with normal glomerular filtration rate. *Hypertension*, **8**, 93–102.
2. Achard, J.M., Disse-Nicodeme, S., Fiquet-Kempf, B. and Jeunemaitre, X. (2001) Phenotypic and genetic heterogeneity of familial hyperkalaemic hypertension (Gordon syndrome). *Clin. Exp. Pharmacol. Physiol.*, **28**, 1048–1052.
3. Wilson, F.H., Disse-Nicodème, S., Choate, K.A., Ishikawa, K., Nelson-Williams, C., Desitter, I., Gunel, M., Milford, D.V., Lipkin, G.W., Achard, J.M. *et al.* (2001) Human hypertension caused by mutations in WNK kinases. *Science*, **293**, 1107–1112.
4. Moriguchi, T., Urushiyama, S., Hisamoto, N., Iemura, S., Uchida, S., Natsume, T., Matsumoto, K. and Shibuya, H. (2005) WNK1 regulates phosphorylation of cation-chloride-coupled cotransporters via the STE20-related kinases, SPAK and OSR1. *J. Biol. Chem.*, **280**, 42685–42693.
5. Vitari, A.C., Deak, M., Morrice, N.A. and Alessi, D.R. (2005) The WNK1 and WNK4 protein kinases that are mutated in Gordon's hypertension syndrome phosphorylate and activate SPAK and OSR1 protein kinases. *Biochem. J.*, **391**, 17–24.
6. Chiga, M., Rafiqi, F.H., Alessi, D.R., Sohara, E., Ohta, A., Rai, T., Sasaki, S. and Uchida, S. (2011) Phenotypes of pseudohypoaldosteronism type II caused by the WNK4 D561A missense mutation are dependent on the WNK-OSR1/SPAK kinase cascade. *J. Cell. Sci.*, **124**, 1391–1395.
7. Yang, S.S., Morimoto, T., Rai, T., Chiga, M., Sohara, E., Ohno, M., Uchida, K., Lin, S.H., Moriguchi, T., Shibuya, H. *et al.* (2007) Molecular pathogenesis of pseudohypoaldosteronism type II: generation and analysis of a Wnk4(D561A/+) knockin mouse model. *Cell. Metab.*, **5**, 331–344.
8. Bergaya, S., Faure, S., Baudrie, V., Rio, M., Escoubet, B., Bonnin, P., Henrion, D., Loirand, G., Achard, J.M., Jeunemaitre, X. *et al.* (2011) WNK1 regulates vasoconstriction and blood pressure response to {alpha}1-adrenergic stimulation in mice. *Hypertension*, **58**, 439–445.
9. Vidal-Petiot, E., Elvira-Matelot, E., Mutig, K., Soukaseum, C., Baudrie, V., Wu, S., Cheval, L., Huc, E., Cambillau, M., Bachmann, S. *et al.* (2013) WNK1-related familial hyperkalemic hypertension results from an increased expression of L-WNK1 specifically in the distal nephron. *Proc. Natl Acad. Sci. USA*, **110**, 14366–14371.
10. Castañeda-Bueno, M., Cervantes-Pérez, L.G., Vázquez, N., Uribe, N., Kantesaria, S., Morla, L., Bobadilla, N.A., Doucet, A., Alessi, D.R. and Gamba, G. (2012) Activation of the renal Na+:Cl- cotransporter by angiotensin II is a WNK4-dependent process. *Proc. Natl Acad. Sci. USA*, **109**, 7929–7934.
11. Rafiqi, F.H., Zuber, A.M., Glover, M., Richardson, C., Fleming, S., Jovanović, S., Jovanović, A., O'Shaughnessy, K.M. and Alessi, D.R. (2010) Role of the WNK-activated SPAK kinase in regulating blood pressure. *EMBO Mol. Med.*, **2**, 63–75.
12. Yang, S.S., Lo, Y.F., Wu, C.C., Lin, S.W., Yeh, C.J., Chu, P., Sytwu, H.K., Uchida, S., Sasaki, S. and Lin, S.H. (2010) SPAK-knockout mice manifest Gitelman syndrome and impaired vasoconstriction. *J. Am. Soc. Nephrol.*, **21**, 1868–1877.
13. Lin, S.H., Yu, I.S., Jiang, S.T., Lin, S.W., Chu, P., Chen, A., Sytwu, H.K., Sohara, E., Uchida, S., Sasaki, S. *et al.* (2011) Impaired phosphorylation of Na(+)-K(+)-2Cl(-) cotransporter by oxidative stress-responsive kinase-1 deficiency manifests hypotension and Bartter-like syndrome. *Proc. Natl Acad. Sci. USA*, **108**, 17538–17543.
14. Susa, K., Kita, S., Iwamoto, T., Yang, S.S., Lin, S.H., Ohta, A., Sohara, E., Rai, T., Sasaki, S., Alessi, D.R. *et al.* (2012) Effect of heterozygous deletion of WNK1 on the WNK-OSR1/ SPAK-NCC/NKCC1/NKCC2 signal cascade in the kidney and blood vessels. *Clin. Exp. Nephrol.*, **16**, 530–538.
15. Boyden, L.M., Choi, M., Choate, K.A., Nelson-Williams, C.J., Farhi, A., Toka, H.R., Tikhonova, I.R., Bjornson, R., Mane, S.M., Colussi, G. *et al.* (2012) Mutations in kelch-like 3 and cullin 3 cause hypertension and electrolyte abnormalities. *Nature*, **482**, 98–102.
16. Louis-Dit-Picard, H., Barc, J., Trujillano, D., Miserey-Lenkei, S., Bouatia-Naji, N., Pylypenko, O., Beaurain, G., Bonnefond, A., Sand, O., Simian, C. *et al.* (2012) KLHL3 mutations cause familial hyperkalemic hypertension by impairing ion transport in the distal nephron. *Nat. Genet.*, **44**, 456–460, 456–460.
17. Kigoshi, Y., Tsuruta, F. and Chiba, T. (2011) Ubiquitin ligase activity of Cul3-KLHL7 protein is attenuated by autosomal dominant retinitis pigmentosa causative mutation. *J. Biol. Chem.*, **286**, 33613–33621.

Downloaded from http://hmg.oxfordjournals.org/ at Tokyo Medican and Dental University on April 13, 2015